

Chapter 1

Preparations

This chapter reviews the fundamental material properties of shape memory alloys and thereby sets up the physical situation our modelling is referring to. Laboratory observations reveal scale-specific characteristics the modelling must reflect. Therefore, shape memory alloys are a prime example of cross-scale modelling. We briefly explain the respective modelling approaches to place the method of molecular dynamics simulations into the scope of the scientific frame work.

1.1 An Introduction to Shape Memory Alloys

1.1.1 Thermo-Mechanical Phenomena

If a material has the ability to recover a large, remaining deformation by undergoing a change in temperature, it is called a shape memory material. This behaviour is observed for different materials, metallic as well as non-metallic. This work is concerned with the memory effect in shape memory alloys (SMA). It was first observed in $\text{Au}_{47.5}\text{Cd}$ by Chang and Read [1] in 1951. Subsequent to this, it was reported for several other alloys, such as Ti–Ni (1963) [2, 3], In–Ti (1953) [4], Cu–Zn (1956) [5–7] and Cu–Al–Ni (1957) [8]. Such alloys characteristically exhibit a strong-temperature dependent stress/strain relation.

Figure 1.1 shows process diagrams which illustrate the thermo-mechanical properties of the specific SMA nickel-titanium. (a)–(c) shows three load–strain isotherms, measured for the temperatures $T_1 < T_2 < T_3$. All curves exhibit significant yielding deformation if the sample is loaded beyond its yield point P_{crit} . These points depend on the temperature, $P_{\text{crit}}(T_1) < P_{\text{crit}}(T_2) < P_{\text{crit}}(T_3)$. Upon unloading, the material's response differs, again depending on the temperature: at higher temperatures, T_2 or T_3 , the deformation recovers at almost constant recovery loads P'_{crit} , while at lower temperatures T_1 no recovery is observed. Rather, the completely unloaded sample exhibits the remaining deformation ε' . Below, as well as above the T-specific yield

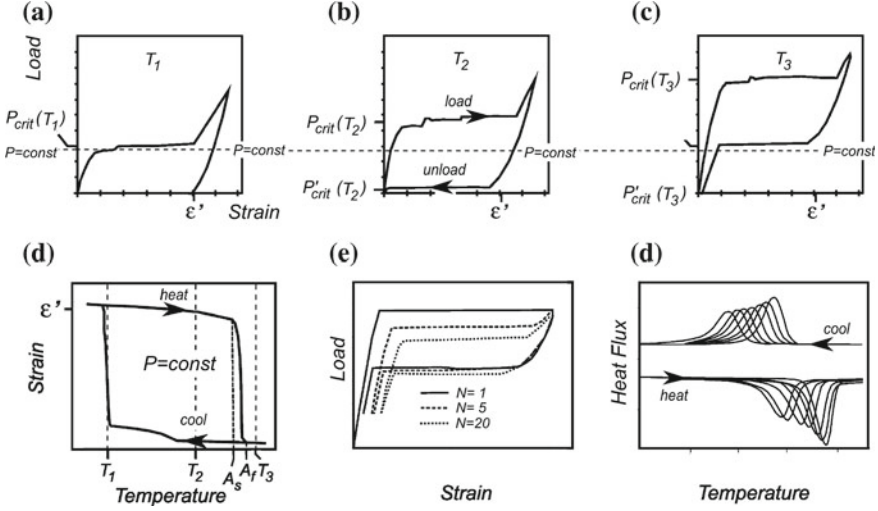


Fig. 1.1 Macroscopic phenomena with SMA. **a–c** Three load–strain isotherms of a NiTi wire. **d** The corresponding strain–temperature relation for load $P = \text{const}$. (Courtesy of Musolf [9]). **e** Tensile cycling of a pristine NiTi specimen. **f** Thermal cycling in a DSC device, where phase transformations are indicated by deviations from the base line signals. The upper array of curves refers to austenite/martensite transformations during cooling and the lower one to reverse processes during heating. (Courtesy of Wagner and Frenzel [10])

and recovery loads, the sample is elastic within certain ranges. The high temperature load–strain response is called pseudo-elastic and that at low temperature is called pseudo-plastic.

The strain–temperature diagram of Fig. 1.1d may be derived from a set of load–strain isotherms by evaluation at a selected constant load. It is obtained from the load–strain curves in (a)–(c) for the constant load $P = \text{const}$. indicated. The strain–temperature diagram (d) may be used to explain the the shape memory effect (SME): subject to the tensile load P , the sample is pseudo-plastically deformed at low temperature T_1 to the strain ϵ' . The sample recovers shape if heated beyond the critical temperature $T = A_f$ in Fig. 1.1d. At high temperatures T_3 , the sample is only slightly strained, corresponding to the applied load remaining constant during the heating, and this strain may be further recovered elastically, if the sample is unload at this temperature (not shown). This observation conveys the impression that the alloy “remembered” its reference shape, thus suggesting the material’s name.

Unfortunately—from an engineer’s viewpoint—the process diagrams of SMAs exhibit hysteresis. In general, the width of the hysteresis loops depend on the specific alloy under consideration and on the processing of the sample. Loading direction also has an impact on the hysteresis behaviour, especially in single-crystalline samples. Some materials may exhibit vanishing hysteresis with $P_{crit}(T) \approx P'_{crit}(T)$. However, the situation can become even worse: the material’s hysteresis appears to depend on the history of the processes performed on it. Transformation loads and

transformation temperatures change during cyclic mechanical or thermal loading. This effect is augmented for pristine materials following casting/heat treatment, but it also affects their long-term service properties. Material scientists subsume such behaviour under the terminology *functional fatigue* [11–14] because of its detrimental effect on material reliability in technical applications. Figure 1.1 illustrates this property during (e) mechanical cycling (20 load cycles) and (f) thermal cycling, as observed with a NiTi sample.

1.1.2 Martensitic Transformations

The SME is based on a special class of solid-solid phase transformations called *martensitic transformations* (MT). These occur in crystalline materials between two fundamental lattice structures called austenite and martensite [15–18]. Austenite forms highly symmetric unit cells which are stable at high temperature. During a MT, the austenitic lattice undergoes a shear and or a shear/shuffle type of transformation and forms martensite which has a lesser degree of symmetry. Variants of martensite exist, basically because there are different deformation modes of the austenitic lattice. Martensite is stable at low temperature, such that lattice transformations may be induced by lowering the temperature below certain transformation temperatures (temperature induced MT). At high temperatures, where austenite is stable, MT may be also induced by applying external loads.

The investigation of MT has a long tradition. It can be traced back to early observations in the 19th century of *martensitic microstructures* in steel—the eponym is Adolf Martens — and has produced a vast literature. An internet inquiry yields a total of 11,488 hits on the Boolean keyword combination (“martensitic transformation” or “martensitic microstructure”) and “shape memory” for the period 1955–2008 [41]. Figure 1.2 depicts this research activity.¹ Notwithstanding this, a final definition of MT which is accepted by all scientists on the field is still overdue. Vivid discussions on this topic are documented in the literature. As late as 1995, the International Conference on Martensitic Transformations (ICOMAT) included a panel discussion, where P.C. Clapp presented a review of past definitions under the provocative title “How would we recognise a martensitic transformation if it bumped into us on a dark & austy night?” His own “irreducible” conjecture was: “A martensitic transformation involves a cooperative motion of atoms across an interface causing a shape change and sound” [42]. The constituents of other definitions were

- MT is diffusion-less and entails a cooperative movement of atoms, leading to a change in shape of the entire body,
- during MT, nearest atomic neighbours remain nearest neighbours,
- MT involves growth processes,
- MT exhibits undistorted, straight interfaces between the parent and the product phase,

¹ The diagram also nicely reveals an inflationary increase in publications in the internet age.

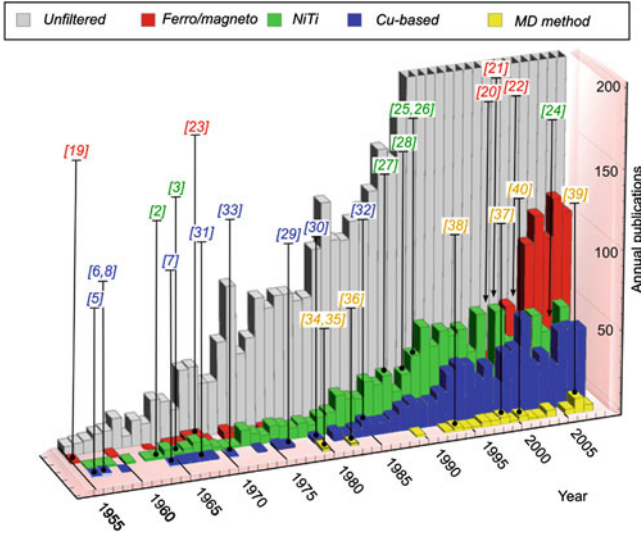


Fig. 1.2 Research activity on shape memory alloys and martensitic transformations 1955–2008. Internet database queries for publications with Boolean keyword combinations of (“martensitic transformation” or “martensitic microstructure”) and “shape memory” in the title (grey, cut-off above 200 hits/year). Additional filter settings with respect to specific materials, yield the coloured columns. The labels [5...40] reference pioneering and most cited works. Note only 46 works match a combinatorial query with respect to (“molecular dynamics” or “atomistic methods”).

- MT includes orientation relationships between principle directions of the lattices involved.

Olson’s definition summarises most of these constituents and is generally accepted today: MT is a shear dominant, lattice distortive, diffusion-less transformation occurring by nucleation and growth [43].

1.1.3 Microstructures

A twinned microstructure is a characteristic of martensite. Twins are martensite variants which are crystallographically compatible along their interface and energetically equivalent. The formation dynamics are complex and yield characteristic, twinned domain structures. Figures 1.3, 1.4 and 1.5 show examples from the centimetre down to the nano scale of lengths.

The martensitic morphology is distinctively recognised in copper based SMA. Figure 1.3 shows observations with a CuNiAl single crystal. On the centimetre scale (a,b), martensite forms wedge-shaped domains by nucleation and growth. If the sample is polished in the austenitic phase, the wedges produce tangible surface textures: the flanks of the wedges in (b) are slightly tilted such that they protrude from the plane

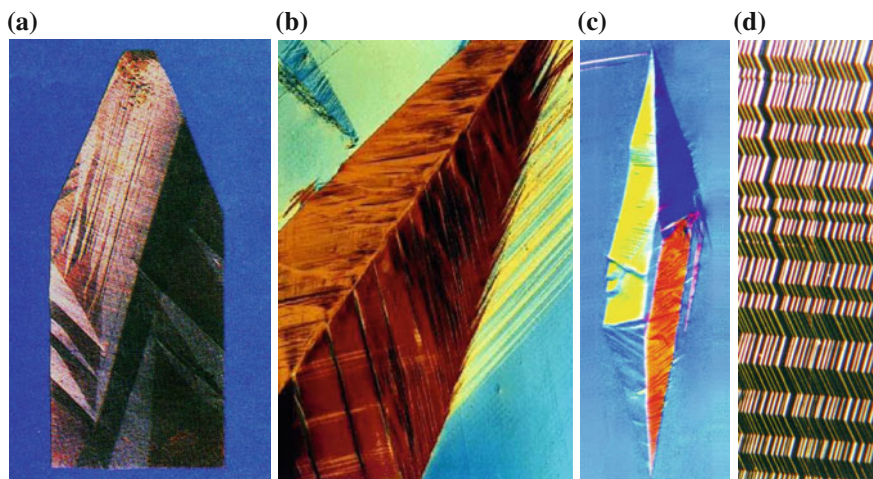


Fig. 1.3 Martensite in a CuNiAl single crystal plate. **a** Temperature-induced wedge-shaped martensitic domains. Centimetre-scale. **b** Low magnification ($16.5\times$) of a single wedge (orange). **c** Four-sided nucleus of compatible variants which belong to the same plate group. Magnification $100\times$. **d** Regular stacks of twins. Magnification $200\times$ [44]

by a small angle. The angle is not arbitrary, rather it is dictated by the crystallographic compatibility condition between parent and product phases. Their interface, called the habit plane, is macroscopically sharp and planar. Fiducial scratches, tagged on a sample in the parent phase, remain piecewise linear in the product phase. A similar compatibility relation holds between martensite twin variants. Compatible variants form *plate groups*. Fig. 1.3 (c) shows a martensite nucleus that consists of four variants belonging to the same plate group. Twinned structures are produced during self-accommodation processes while martensite is formed. The product exhibits a lamellar structure of regularly stacked, alternating twin variants. These can be observed by optical microscopy at the sub-millimetre scale in Cu-based alloys, Fig. 1.3(d), but are also reflected on much smaller scales, see below.

Figure 1.4 illustrates how martensite wedges are macroscopically formed in a CuNiAl single crystal, showing a series of snapshots obtained from a differential image correlation (DIC) study. The material is the same as in Fig. 1.3. DIC traces the evolution of surface deformations by means of a computer-aided analysis of digital images taken continuously during the process. For this purpose, the sample needs to be coated with a tracer paint. Using stereographic projection, the method yields all components of the transformation surface strains. Figure 1.4a shows the MT nucleation at a singular point at the plate edge. It forms a wedge by a growth process into the bulk material (b)–(c). Eventually, more nuclei appear at other loci and grow, producing a diverse martensite structure (d). The final product (not shown) is similar to the one of Fig. 1.3a.

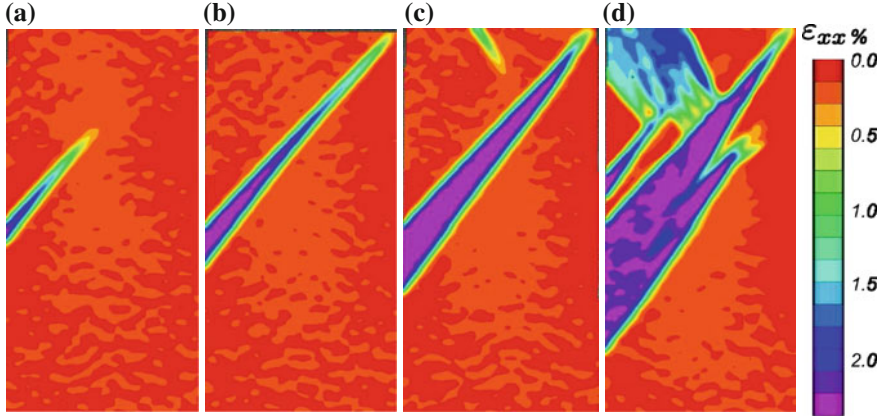


Fig. 1.4 Four consecutive snapshots during a DIC observation of the nucleation and growth of martensite wedges in an austenitic CuNiAl single crystal plate. Plate dimensions $50 \times 25 \times 3$ mm. Colours code the transformation strains ε_{xx} with respect to the austenitic reference configuration (red/orange). Martensite plates exhibit almost homogeneous strains (purple). Note the significant strain gradient field around the wedges. Ref. [45] with courtesy of Musolf for providing the sample (Video available online)

Transmission electron microscopy (TEM) reveals the structure of martensite down to the atomic length scale. Figure 1.5 presents images of various materials from the micro- to the nanometric scale. NiTi (a, c) has a comparatively small-sized domain structure. The two images in (a) and (c), show the characteristic twin lamella of martensite in this alloy. In the case of (c), the martensitic self-accommodation process has produced the typical herringbone structure within a small grain. The lamellar morphology is more pronounced in (b) which depicts a TEM image of NiTiFe. The use of high resolution (HR) TEM enables morphologies to be studied even down to the atomic scale, Fig. 1.5d. Here, white dots locate the positions of individual atoms in a NiAl lattice—or rather, the positions of atomic columns oriented in the viewing direction. This image beautifully confirms that locally, MT produces homogeneous deformations within individual lamellae, where the lattice is regular. Thus, the structure must have been produced by regimented atomic movements during the transformation, which inspired the phrase *military transformation*. For this particular example, the lamella widths range between 10 and 20 unit cells. Across the interfaces of the adjacent lamellae, the strain field is discontinues.

1.1.4 Scales

Materials sciences experimentally and theoretically address the properties of materials across a range of length- and times scales. The technical evolution of microscopy and the coming of computational sciences have emphasised this general approach

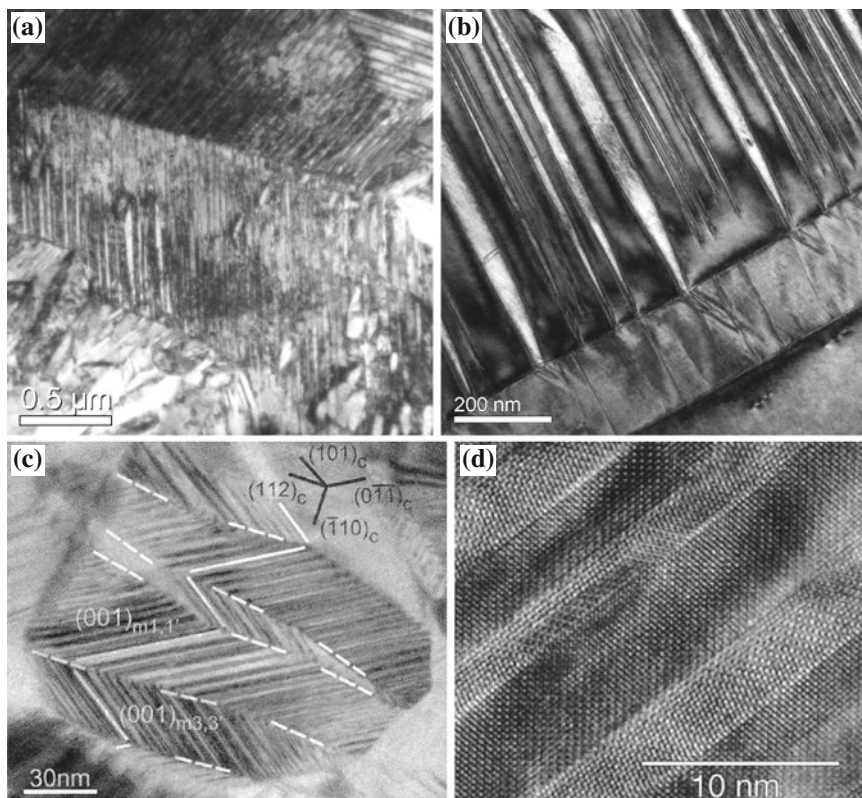


Fig. 1.5 TEM and HR-TEM images of martensite in various SMAs, micro- to nanometre length scale. **a** NiTi, **b** NiTiFe (both images courtesy Ch. Somsen [46]). **c** NiTi [47]. **d** NiAl courtesy D. Schryvers [48]

during the past decade. Shape memory alloy research may well be viewed as a prime example of this. Macroscopic observables are temperature, load and strain. Experiments exhibit a characteristic coupling of these quantities, effectively rationalised by thermodynamics. On the other hand, microscopy unveils complex details of these lattice transformationson at the atomic length scale: product lattices are constituted by (locally homogeneous) transformation strains, governed by coherency constraints to be met along planar phase interfaces. These constraints are met during accommodation processes, forming distinct microstructures. High-resolution transmission electron microscopy is capable of resolving these with atomic detail post-mortem, however, the formation *dynamics* remains experimentally unresolved at this scale level. To understand the dynamics on the atomic scale, we are to rely on theoretical approaches. Here, the micro scale variables are positions and velocities of discrete atoms. These quantities are governed by equations of motion. Still, thermodynamics rules stability, but in this case the stability criterion is determined by atomic vibrations and interaction forces. The forces, however, cannot be measured directly.

In this situation, the sub-atomic scale gains importance, as binding forces between atoms are dependent of the distributions of charged sub-atomic particles, electrons and protons.

Against the background of this complexity, it is easy to see that the physics of shape memory alloys indeed poses a multi-scale problem. The significant time and length scales may be roughly divided into the four categories sub-micro—micro-meso-macro. Each scale employs characteristic times and lengths.

The sub-microscopic level concerns the electronic structure of atomic cores and the related electron distributions. These are investigated by means of *ab initio* models and quantum mechanics. On the microscopic level, atoms are considered as mass-points in the mathematical sense. Based on semi-empirical interaction-functions given, formations of lattice structures can be investigated by molecular dynamics simulations and, statically, by relaxation methods. Characteristic times and lengths are the period of an atomic oscillation (≈ 1 fs) and a lattice constant (≈ 1 Å), respectively. Processes accessible by these methods range up to nano seconds and micro metres. The mesoscopic scale level is somewhat ambiguously positioned between micro and macro and concerns characteristic microstructural entities having the capability of influencing the macroscopic material properties as ensembles. Examples are martensite lamellae, precipitates, inclusions, dislocations, grains and domains. Mesoscopic entities have characteristic lengths from nanometres up to micrometres. The characteristic time may be defined with respect to the speed of sound. Mesoscale processes are accessible by both atomistic and continuum methods (“*micro-mechanics*”), thus opening up the opportunity of transferring information between these two modelling techniques.

Above the mesoscopic level, matter is considered to be macroscopically continuous and the classical continuum theories of mechanics and thermodynamics are applied. A typical numerical tool used for computing the continuum-level field equations is the finite element method (FEM).

While each scale incorporates complex theories and sophisticated mathematical toolsets of own rank, additional challenges arise from the need of bridging information between the scale, since different, scale-specific sets of variables are used. For example, atomic interaction forces on the micro scale depend on charge distributions resolved on the submicro-scale. These, however, are not represented on the micro scale. Similarly, constitutive equations are required as function of the thermo-mechanical field variables on the macro-scale, whereas the microscale concerns velocities and positions of atoms. Bridging between the scales is a classical problem and has been tackled since long. Cauchy, for example, derived the elasticity tensor of a monatomic solid in 1890 based on assumptions on the atomic interactions. His work has yielded restrictive relations on the number of independent elastic constants [49] which, however, were later experimentally disproved. These *Cauchy relations* are therefore today regarded as a negative test for the reliability of an atomic interaction model.² Another, most important classical scale-bridging method was contributed

² Note in 1915, Born was able to prove the Cauchy relations do not apply in the case of nested, many-species lattices owing to the contributions from interactions between the sublattices [50].

within the framework of statistical thermodynamics by Maxwell and Boltzmann. Boltzmann's statistical interpretation of the entropy for an ideal gas was quickly extrapolated to condensed matter; his approach still represents the only theoretical method of rationalising entropy and all related thermodynamic quantities from first principles. For this reason his famous formula $S = k \log W$ ranges among the most important equations of all physics [51].

1.2 Crystallographic Theory

The crystallographic theory of martensite [15, 16, 18, 52–56] relies on two phenomenological macroscopic observations: First, austenite-martensite phase boundaries appear as invariant *habit planes*, which are sharp, non-rotated and undistorted. Second, linear fiducial scratches remain piecewise linear after the transformation. From these two observations it can be concluded that, macroscopically, the deformation gradient \mathbf{F} may be expressed by

$$\mathbf{F} = \mathbf{I} + \mathbf{d} \otimes \mathbf{p} \quad (1.1)$$

(\mathbf{p} —normal to the habit plane, \mathbf{d} —arbitrary vector, \mathbf{I} —identity matrix). Microscopically, the deformation gradient can be represented by a combination of the Bain transformation $\mathbf{B}(\eta_1, \eta_2, \eta_3)$, simple shear $\mathbf{P}(s)$ and rotations $\mathbf{R}(\alpha, \beta, \gamma)$,

$$\mathbf{F} = \mathbf{R}\mathbf{P}\mathbf{B}. \quad (1.2)$$

The Bain transformation incorporates changes in the lattice parameters (η_1, η_2, η_3) during the transformation. This is illustrated in Fig. 1.6. The lattice parameters can, in principle, be measured by X-ray methods and thus are taken as given in this theory. The shear is indicated by a scalar shear parameter s and the rotation by the three Eulerian angles (α, β, γ). Both shear and rotation are required to compatibly “fit” the product to the parent along a habit plane.

Equations (1.1) and (1.2) establish a nine-dimensional algebraic system for determining the components of \mathbf{d} and \mathbf{p} ; the rotations and the shear as functions of the Bain parameters ($|\mathbf{p}| = 1$ serves as implicit condition). This system is non-linear, thus multiple solutions exist which indicate martensite variants. Among these variants, not all pairings are compatible such that martensite twins form. Twins are formed by pairs of compatible variants \mathbf{F} and $\tilde{\mathbf{F}}$ that obey the twinning condition

$$\mathbf{F} - \tilde{\mathbf{F}} = \mathbf{a} \otimes \mathbf{m} \quad (1.3)$$

along their interface (\mathbf{m} —normal to that interface, \mathbf{a} —arbitrary vector). This condition holds if one of the two following conditions is satisfied: either the deformation

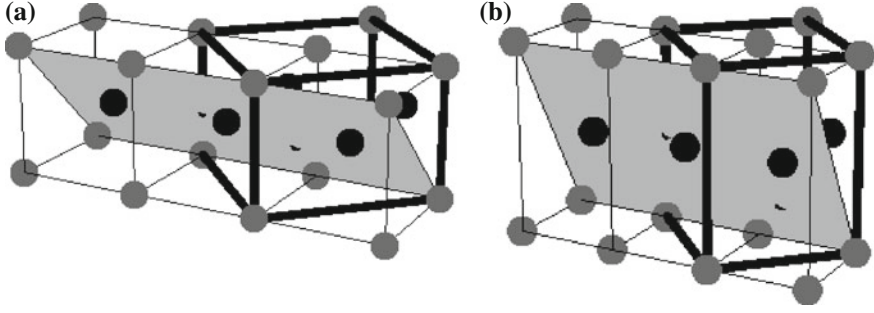


Fig. 1.6 Bain transformation of a body-centred-cubic (bcc) lattice. The cubic parent lattice (a) may be alternatively described by primitive bcc unit cells (thin lines) or by face-centred-tetragonal (fct) unit cells (bold lines). The Bain transformation stretches the fct lattice homogeneously along one cell axis and compresses it along the other two, thus producing a deformed fct cell in the product lattice (b), while the bcc parent cells deform into bct product cells. The Bain parameters (η_1, η_2, η_3) indicate the ratios of the fct unit cell edge lengths in the two structures. During this process, the plane $(011)_{\text{bcc}}$ is slightly rotated so as to become the product plane $(011)_{\text{bct}}$ which is close-packed

vectors \mathbf{d} and $\tilde{\mathbf{d}}$ or the habit plane normals \mathbf{p} and $\tilde{\mathbf{p}}$ of the variant pair concerned are parallel.³

$$\text{Kinematic compatible martensites: } \mathbf{d} \parallel \tilde{\mathbf{d}} \vee \mathbf{p} \parallel \tilde{\mathbf{p}}. \quad (1.4)$$

To model the lamellar microstructure of martensite, energetic arguments were introduced. The concept by James and Ball [57] follows the idea that the microstructure may be represented by a sequence of piecewise homogeneous deformations $y^i(x)$ which obey the crystallographic conditions. The microstructure is determined by minimising the total free energy F in a domain Ω ,

$$F = \int_{\Omega} f(\mathbf{F}(y^i)) dx + \sigma A(i) \rightarrow \min!, \quad (1.5)$$

where the specific free energy f is represented by the elastic strain energy of the sequence. The term $\sigma A(i)$ represents the interface energy between martensitic vari-

³ Proof following I. Müller in three steps:

1. Suppose $\mathbf{d} \parallel \tilde{\mathbf{d}}$, that is $\tilde{\mathbf{d}} = \alpha \mathbf{d}$, where α is a real scalar. Hence $\mathbf{F} - \tilde{\mathbf{F}} = \mathbf{d} \otimes (\mathbf{p} - \alpha \tilde{\mathbf{p}})$ and we conclude that the condition (1.3) holds for $\mathbf{a} = \mathbf{d}$ and $\mathbf{m} = \mathbf{p} - \alpha \tilde{\mathbf{p}}$.
2. Suppose $\mathbf{p} \parallel \tilde{\mathbf{p}}$, that is $\tilde{\mathbf{p}} = \beta \mathbf{p}$, where β is a real scalar. Hence $\mathbf{F} - \tilde{\mathbf{F}} = (\mathbf{d} - \beta \tilde{\mathbf{d}}) \otimes \mathbf{p}$ and we conclude that the condition (1.3) holds for $\mathbf{a} = \mathbf{d} - \beta \tilde{\mathbf{d}}$ and $\mathbf{m} = \mathbf{p}$.
3. Now suppose that the two vectors \mathbf{p} and $\tilde{\mathbf{p}}$ are not parallel, $\mathbf{p} \nparallel \tilde{\mathbf{p}}$. Thus the normal vector \mathbf{m} may be represented as a linear combination of \mathbf{p} and $\tilde{\mathbf{p}}$, $\mathbf{m} = \alpha \mathbf{p} + \beta \tilde{\mathbf{p}}$, where α, β are real scalars. It follows from (1.3) that $\mathbf{d} \otimes \mathbf{p} - \tilde{\mathbf{d}} \otimes \tilde{\mathbf{p}} = \mathbf{a} \otimes (\alpha \mathbf{p} + \beta \tilde{\mathbf{p}})$, or, after re-arranging $(\mathbf{d} - \alpha \mathbf{a}) \otimes \mathbf{p} = (\tilde{\mathbf{d}} - \beta \mathbf{a}) \otimes \tilde{\mathbf{p}}$. This condition implies the vectors \mathbf{d} and $\tilde{\mathbf{d}}$ must be parallel in this case, since $\mathbf{d} = \alpha \mathbf{a}$ and $\tilde{\mathbf{d}} = \beta \mathbf{a}$ are the only choices which meet the condition (1.3). With this result, we may now return to 1, which concludes the proof of the statement (1.4).

ants and it scales proportionally with the number of interfaces. *Without* the interface term, the variational Eq. (1.5) yields an unrealistic, infinitely fine microstructure, while finite-sized microstructures are generated if the interface energy is taken into consideration: The strain energy term in Eq. (1.5) delimits only a few interfaces while the interface term represses many interfaces. Thus when both terms are present, their effects mediated each other and they yield a finite-sized microstructure. A related variational model considers smooth energy functions and the interface energies are modelled as proportional to the square of the second derivative $y''(x)$ [58–64]. Yet another related concept considers homogeneous phase mixtures and introduces phase field variables controlled by a set of Langevin type equations [65, 66]. Here again, strain gradients represent interface energies.

Kinetic aspects of phase transformations in solids were investigated separately by continuum methods [67–69], however, such work focuses on the thermodynamics of transformation shocks in one-dimensional settings whereby the microstructural detail is lost.

1.3 Thermodynamics

1.3.1 Phase Stability Criterion

The stability of a physical system is a subject of thermodynamics. If a system is exposed to non-equilibrium conditions, transport processes result which adjust the system variables. Such processes are described by the thermodynamic field theory. Continuum-scale field variables are defined, typically the fields of (partial) density, the motion related variables (partial) velocity and strain and temperature. These quantities must obey the local balance laws of (partial) mass, (partial) momentum and energy in all regular material points, and their respective jump conditions at singular surfaces. These balance equations incorporate a range of additional physical quantities called the “constitutive” equations—caloric and thermal equations of state, heat flux and diffusion flux, etc.—which must be determined as functions of the field variables in order to constitute a closed mathematical system of equations. Experiments reveal these functions exhibit material-specific dependencies of the field variables and their determination is subject of the thermodynamic materials theory. Thermodynamics axiomatically sets up an important constraint on the constitutive equations, called the “entropy principle”. This principle is constituted by the entropy balance, which represents an inequality: Entropy is not conserved during a thermodynamic process, rather than it experiences production which is non-negative by any experience [70].

Therefore, the entropy principle defines the “direction” of relaxation processes into equilibrium states, which are characterised by the phase equilibrium, the mechanical equilibrium and the thermal equilibrium. To see this we focus attention to the integral balance equations of mass, energy and entropy which we specify for the

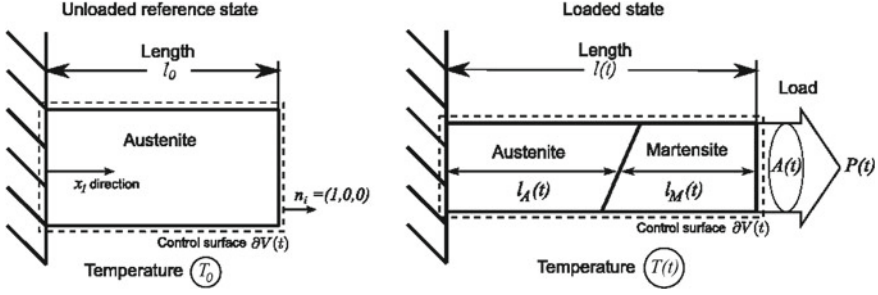


Fig. 1.7 Sketch on the phase stability criterion. A uni-axially applied load P affects the current length $l(t)$ effecting work at a rate $P dl/dt$ across the control surface

situation of a specimen under axial tensile load, cf. Fig. 1.7, in order to derive and investigate these thermodynamic equilibrium criteria. For details we refer to textbooks [71]; our presentation of the matter further benefits from the studies of [72–75].

The balance equations for mass, energy and entropy of the specimen under axial tensile load of Fig. 1.7 read

$$\frac{dm}{dt} = 0 \rightarrow m_M(t) = m - m_A(t), \quad (1.6)$$

$$\frac{d(U + K)}{dt} = \dot{Q} + \oint_{\partial V(t)} t_{ij} v_i n_j dA, \quad (1.7)$$

$$\frac{dS}{dt} \geq \frac{\dot{Q}}{T}. \quad (1.8)$$

We consider a specimen of mass m which may decompose into generic phases austenite (A) and martensite (M). The partial masses are m_A and m_M . The total mass is conserved, Eq. (1.6)₁, hence these partial masses are related, Eq. (1.6)₂.

The energy balance (1.7) states the change of the total energy—the sum of the internal energy U and the kinetic energy K —results from heat exchange \dot{Q} with the ambience and from external working. Here we neglect working effected by body forces like gravitation or external magnetic fields in order to focus on the effect of tensional forces acting across the control surface $\partial V(t)$. These are represented by Cauchy stress t_{ij} acting on surface elements dA at the local velocities v_i . These surface elements are oriented by normal vectors n_j .

The surface integral on the right-hand side of Eq. (1.7) may be simplified to a tangible expression employing some assumptions: As of Fig. 1.7, tensions are only acting across the surface segments to the left and right of the tensile specimen. To the left, it is rigidly fixed and the surface velocities are locally zero, $v_i = 0$. To the right-hand side—the loading side—the velocity of the surface is $v_i = (dl(t)/dt, 0, 0)$ and only axial tensions are applied, which are effected by a nominal force $P(t)$. Here, the surface has the size $A(t)$ and the normal vector is $n_i = (1, 0, 0)$. Hence the axial

surface stress component reads $t_{11} = P(t)/A(t)$. In this simple situation the surface integral in Eq. (1.7) reduces to

$$\oint_{\partial V(t)} t_{ij} v_i n_j dA = \int_{A(t)} \begin{pmatrix} \frac{dl(t)}{dt} \\ 0 \\ 0 \end{pmatrix}^T \begin{pmatrix} \frac{P(t)}{A(t)} & 0 & 0 \\ 0 & 0 & 0 \\ 0 & 0 & 0 \end{pmatrix} \begin{pmatrix} 1 \\ 0 \\ 0 \end{pmatrix} dA = P(t) \frac{dl}{dt}. \quad (1.9)$$

We consider slow processes, where the changes of the kinetic energy K may be neglected. Further we assume the heat exchange \dot{Q} with the ambience occurs at a homogeneous surface temperature T . The entropy S of the specimen according to Eq. (1.8) then changes due to the heat exchanged at that temperature and by a—here not further specified—entropy production rate, which is non-negative. By eliminating the heat flux from Eqs. (1.7) and (1.8), and applying a Legendre Transformation, the stability criterion is furnished:

$$\frac{d}{dt} (U - TS - Pl) \leq -S \frac{dT}{dt} - l \frac{dP}{dt}. \quad (1.10)$$

This criterion states for fixed external load P and fixed surface temperature T , the rate of the Gibbs free enthalpy $G \equiv U - TS - Pl$ is negative such that it eventually becomes minimal at equilibrium. This minimum-condition is a direct consequence of the entropy inequality.

A few re-arrangements are useful. Conventionally, the absolute axial length $l(t)$ of the specimen is substituted by the strain $\varepsilon = (l - l_0)/l_0$, where $l_0(T_0, P = 0)$ denotes a reference length. In the framework of SMA, the reference state is typically unloaded austenite at a reference temperature T_0 , where this phase is stable. In this state the loading surface has the area A_0 and $\rho_0 = m(l_0/A_0)$ denotes the mass density in the reference state. The phase specific strains are ε_A and ε_M . These are defined for austenite and martensite with $l = l_A$ and $l = l_M$, respectively.

The Cauchy stress t_{ij} in Eq. (1.7) refers to the current area $A(t)$. Alternatively, we may relate the applied forces $P(t)$ to the reference area A_0 and define the (first) Piola–Kirchhoff stress component $\sigma = P/A_0$.

Finally, we may introduce mass-specific quantities of energy and entropy, $u = U/m$ and $s = S/m$. The phase-specific equivalents of these quantities are $u_{A,M} = U_{A,M}/m_{A,M}$ and $s_{A,M} = S_{A,M}/m_{A,M}$, respectively. Employing these definitions, the mass specific total free enthalpy reads $g = u - Ts - \sigma\varepsilon/\rho_0$. The mass-specific free enthalpies are defined as $g_A = u_A - Ts_A - \sigma\varepsilon_A/\rho_0$ for the austenite and $g_M = u_M - Ts_M - \sigma\varepsilon_M/\rho_0$ for the martensite, respectively.

According to Eq. (1.10) has the total free enthalpy a minimum at equilibrium. Employing all the new quantities defined above, a global equilibrium state hence is characterised by the condition

$$\frac{d}{dt} (m_A g_A(T, \sigma) + (m - m_A) g_M(T, \sigma)) = 0. \quad (1.11)$$

The mass balance (1.6)₂ was evaluated to eliminate m_M . Equation (1.11) therefore depends on the three independent variables m_A , T and σ , implying three necessary conditions for global equilibrium:

$$\left(\frac{\partial g}{\partial m_A}\right)_{T,\sigma} = 0, \quad \left(\frac{\partial g}{\partial T}\right)_{m_A,\sigma} = 0, \quad \left(\frac{\partial g}{\partial \sigma}\right)_{T,m_A} = 0. \quad (1.12)$$

These are the conditions for the phase equilibrium, the thermal equilibrium and the mechanical equilibrium, respectively. Especially, Eq. (1.12)₁ implies

$$\left(u_A - Ts_A - \frac{\sigma \varepsilon_A}{\rho_0}\right) \Big|_E = \left(u_M - Ts_M - \frac{\sigma \varepsilon_M}{\rho_0}\right) \Big|_E. \quad (1.13)$$

The index “E” reminds us this equation refers to an equilibrium state.

The phase equilibrium condition (1.13) relates the phase transformation load $\sigma(T)$ and the phase transformation temperature $T(\sigma)$. Their dependency is expressed by the Clausius–Clapeyron equation:

$$\frac{d\sigma}{dT} = \rho_0 \frac{s_A - s_M}{\varepsilon_M - \varepsilon_A}. \quad (1.14)$$

This relation is directly obtained from Eq. (1.13) by resolving it σ and subsequent derivation with respect to T .

Experiments reveal that under tensional loading, the transformation stress of austenite/martensite transformations $\sigma(T)$ is always increasing with temperature. So the right-hand side of Eq. (1.14) must be positive. The strain difference ($\varepsilon_M - \varepsilon_A$) in the denominator on the right-hand side of this equation represents the transformation strain and this quantity also is positive, since the strains refer to an austenitic reference state. In order to meet the experimental observation, Eq. (1.14) therefore requires the difference of the specific entropies ($s_A - s_M$) must be positive too. Accordingly, the specific entropy s_A of austenite must be bigger than the specific entropy of martensite s_M . An atomistic explanation of this condition is given in Sect. 3.2.3.

There are two approaches to graphically evaluate the phase equilibrium condition of Eq. (1.13). These are known as the “rule of equal areas” and the “rule of common tangents”. To see this, we may re-write Eq. (1.10) assuming reversible conditions⁴ to yield the Gibbs Equation,

$$\frac{d(u - Ts)}{dt} = -s \frac{dT}{dt} + \frac{\sigma}{\rho_0} \frac{d\varepsilon}{dt}. \quad (1.15)$$

The combination of internal energy u and entropy s and the left-hand side of this equation defines the mass-specific Helmholtz free energy $f \equiv u - Ts$. We see from

⁴ In thermodynamics, a process is called reversible if the entropy production is zero. In this case the entropy balance (1.8) turns into an equality. In nature no such processes exists, therefore the idea of reversibility must be regarded as an idealisation.

Eq. (1.15) that this free energy is depending on the variables T and ε . Therefore the total differential $df(T, \varepsilon)$ reads

$$\frac{df(T, \varepsilon)}{dt} = \left(\frac{\partial f}{\partial T} \right)_{\varepsilon} \frac{dT}{dt} + \left(\frac{\partial f}{\partial \varepsilon} \right)_T \frac{d\varepsilon}{dt}. \quad (1.16)$$

Comparing the coefficients between Eqs. (1.15) and (1.16) we see that the stress $\sigma(T, \varepsilon)$ is fundamentally related to the free energy under isothermal conditions through

$$\begin{aligned} \frac{\sigma(T, \varepsilon)}{\rho_0} &= \left(\frac{\partial f}{\partial \varepsilon} \right)_T \quad \text{or, with } f \equiv u - TS : \\ \frac{\sigma(T, \varepsilon)}{\rho_0} &= \left(\frac{\partial u}{\partial \varepsilon} \right)_T - T \left(\frac{\partial s}{\partial \varepsilon} \right)_T, \end{aligned} \quad (1.17)$$

Equation (1.17) may be easily extended to all components of the stress tensor, see [76]. We see the stress has both an energetic and an entropic part, as indicated in Eq. (1.17)₂. Both parts are significant in SMA!

Figure 1.8 shows a generic (stress, strain) isotherm in subfigure (a) and the according free energy function in subfigure (b). Note that the (stress, strain) isotherm in (a) is non-monotonous, which corresponds to the non-convexity of the free energy isotherm in (b), since the two graphs are related through Eq. (1.17)₁. Instable branches of these curves are dashed: the stress exhibits a negative slope in this region and the free energy is concave. We may explain the “rule of equal areas” and the “rule of common tangents” using these illustrations.

The “rule of equal areas” represents an interpretation of the phase equilibrium condition (1.13) in the (σ, ε) space. Due to the non-monotonicity of the stress/strain curve in Fig. 1.8a, the stable branches of the stress/strain curve overlap for some stress range. The transformation stress has to be determined within this range. To see this we may re-write Eq. (1.13) employing Eq. (1.17)₁ and yield the expression

$$\int_{\varepsilon_A}^{\varepsilon_M} \sigma(T, \hat{\varepsilon}) d\hat{\varepsilon} = \sigma(T)(\varepsilon_M - \varepsilon_A). \quad (1.18)$$

This equation implies the graphical interpretation visualised in Fig. 1.8a: The phase transformation stress is defined by that specific constant stress line $\sigma(T) = \text{const.}$ which preserves equal sizes of the two areas $\int_{\varepsilon_A}^{\varepsilon_M} \sigma(T, \hat{\varepsilon}) d\hat{\varepsilon}$ and $\sigma(T)(\varepsilon_M - \varepsilon_A)$. Or, equivalently, the grey-shaded areas indicated in that figure are of equal size. The respective transformation stress $\sigma(T)$ line is called the “Maxwell Line”. Below ε_A , the specimen is homogeniously austenitic and it is homogeniously martensitic above ε_M . In these regions the material may be deformed elastically. In the strain range between ε_A and ε_M , austenite-martensite transformations occur

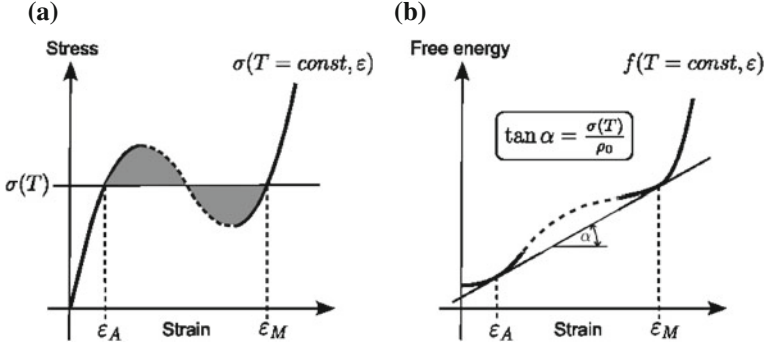


Fig. 1.8 Schematic stress/strain (a) and free energy/strain (b) isotherms. The rule of “equal areas” refers to (a) and the rule of “common tangents” to (b)

upon loading and martensite-austenite transformations occur upon unloading at the same constant stress $\sigma(T)$. Along this stress line, the specimen decomposes into a phase mixture of austenite and martensite such that the Maxwell Line is parametric in the mass-fractions of the phases.

The “rule of common tangents” represents an interpretation of the phase equilibrium condition (1.13) in the (f, ε) space. It represents an alternative interpretation of this condition. To see this, the phase equilibrium condition (1.13) and Eq. (1.17) are combined so as to give the equality

$$\frac{f_A - f_M}{\varepsilon_A - \varepsilon_M} = \frac{\sigma(T)}{\rho_0} = \left(\frac{\partial f}{\partial \varepsilon} \right)_{\varepsilon=\varepsilon_A} = \left(\frac{\partial f}{\partial \varepsilon} \right)_{\varepsilon=\varepsilon_M}. \quad (1.19)$$

This equation implies a graphical interpretation in the (free energy, strain) diagram of Fig. 1.8b: At phase equilibrium, the partial derivatives of the free energy at the loci ε_A and ε_M are equal to both one another and to the transformation stress. This situation may be visualised by a common tangent attached to the respective convex branches of the free energy representing the two phases. The slope of this common tangent determines the phase transformation stress $\sigma(T)/\rho_0$. Again, below ε_A the specimen is homogeneously austenitic and homogeneously martensitic above ε_M . Elastic deformation of the two homogeneous phases is indicated by variations of the free energy within the respective convex wells of $f(\varepsilon, T)$. In between ε_A and ε_M , where the specimen decomposes into a phase mixture of austenite and martensite, the free energy evolves along the common tangent indicated in Fig. 1.8b rather than following the concave branch of the function $f(\varepsilon, T)$. Therefore, by decomposing into a mixture, the specimen “avoids” the energy barrier of the function $f(\varepsilon, T)$ in this strain range. The path along the common tangent, parametrically in the mass-fractions of the phases, therefore is called a “convex hull” of the non-convex free energy in the language of mathematics.

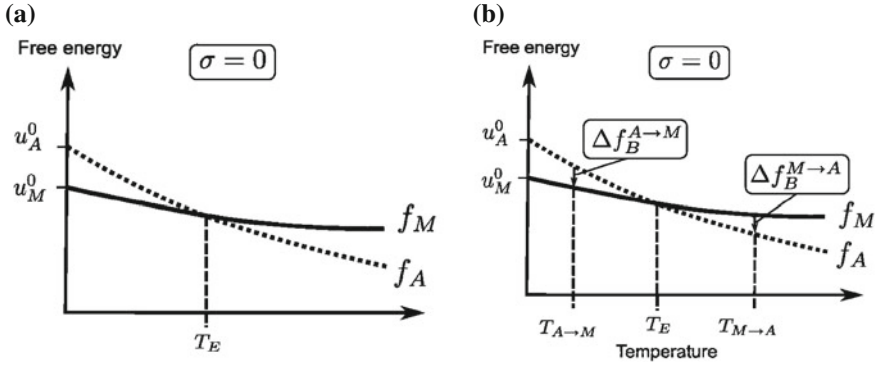


Fig. 1.9 Thermodynamic phase equilibrium criterion for the unloaded specimen. Sketches of the specific free energies of austenite (A) and martensite (M). **a** A unique transformation temperature as predicted by Eq. (1.10). No hysteresis! **b** Experimentally observed situation: Transformation hysteresis between the two observed transformation temperatures $T_{A \rightarrow M}$ and $T_{M \rightarrow A}$

We append an investigation of austenite/martensite transformations for the special situation of zero load, $\sigma(T) = 0$. In this case, the transformation is induced by change of temperature and the equilibrium theory predicts the phase transformation occurs at the specific temperature $T_E = T(\sigma = 0)$. For this special case, the free enthalpies g_A and g_M reduce to the free energies f_A and f_M and the phase equilibrium condition of Eq. (1.13) becomes

$$(u_A(T, \sigma = 0) - T s_A(T, \sigma = 0)) \Big|_E = (u_M(T, \sigma = 0) - T s_M(T, \sigma = 0)) \Big|_E. \quad (1.20)$$

All quantities in this equation refer to a mechanically unloaded state. Therefore, Eq. (1.20) may be used to calculate the phase transformation temperature T_E . An illustrative graphical interpretation of this situation can be given in the (free energy, temperature)-diagram, see Fig. 1.9a. This diagram visualises the two functions $f_A = u_A - T s_A$ and $f_M = u_M - T s_M$ of the unloaded specimen. Both are monotone in temperature and intercept the ordinate at $u_A^0 = u_A(T = 0, \sigma = 0)$ and $u_M^0 = u_M(T = 0, \sigma = 0)$, the respective ground-state energies of the two phases. The slopes of the two free energy functions are given by the entropies ($-s_A(T, \sigma = 0)$) and ($-s_M(T, \sigma = 0)$). These are (roughly) logarithmic functions of temperature but contain phase specific constants responsible for the different slopes of $f_A(T)$ and $f_M(T)$. The intersection of the two functions f_A and f_M determines the transformations temperature T_E .

In the framework of the Clausius–Clapeyron Eq. (1.14) we have already mentioned that phenomenologically, the specific entropy of austenite must be bigger than the one of the martensite, $s_A > s_M$, therefore f_A must be steeper than f_M . In this situation, Eq. (1.20) requires the ground state energy u_M^0 of martensite must be smaller than the ground state energy u_A^0 of austenite, $u_M^0 < u_A^0$, to allow for temperature-induced transformations, see Fig. 1.9a.

Equation (1.20) suggests an interpretation of phase transformations between austenite and martensite in a broader view. Phase transformations in general occur as the result of two competing phase preferences, the ones of energy and of entropy [75]. While seeking for equilibrium, a sample tends to minimise the energy while it tends to maximise entropy at the same time. It turns out these quantities prefer different phases: Martensite produces lattice structures which minimise the internal energy, while the structure of austenite has comparably higher internal energy. This is reflected by the groundstate energies of the two phases. Therefore, martensite is the favourable phase from the energetic perspective. On the other hand, the austenite allows for a bigger specific entropy, than the martensite. Hence, austenite is the preferred phase from the perspective of entropy. Consequently, the phase stability is the result of a competition between the internal energy u and the entropy s , expressed by the free energy $f = u - Ts$. The temperature represents a weighting factor, which determines the influence of entropy. At low temperatures, this influence is diminished, hence allowing the specimen to follow the energetic phase preference. Accordingly, martensite is stable. With increasing temperature, the entropic influence is gradually augmented and eventually dominates. Therefore, austenite is stable at high T . At the phase transformation temperature T_E , energy and entropy are balanced. This mechanism is called “entropic phase stabilisation” of austenite. It represents a general concept in thermodynamics [75]. In the framework of austenite/martensite transformations discussed in this book we will explain this mechanism on the background of an atomistic model.

1.3.2 Nucleation and Hysteresis

The classical thermodynamic treatment of phase transformations in fluids is based on the Gibbs equation and implies process reversibility. Phase stability is determined by the Gibbs free energy for homogeneous bulk matter, resulting in phase diagrams which are hysteresis-free. The Maxwell line in Fig. 1.8 is identical for austenite/martensite transformations as well as for the reverse process. Similarly, a single phase transformation temperature T_E is predicted for an unloaded sample, see Fig. 1.9a. No hysteresis, neither in stress, nor in temperature arises from the thermodynamics theory presented so far. In contrast to this, hysteresis is well observed in the laboratory for both settings. In tensile tests, austenite/martensite transformations are observed at higher transformation stresses upon loading, than upon unloading for the reverse processes. Similarly, two transformation temperatures are detected for unloaded samples in DSC devices between temperatures $T_{M \rightarrow A} > T_E$ and $T_{A \rightarrow M} < T_E$. The widths and shapes of the hystereses depend on the specific alloy, the crystal structure, processing parameters or even specific tensile loading directions. Also, hystereses appear to depend on the history of the processes performed with the material: the transformation stresses and the transformation temperatures change after cyclic mechanical or thermal loading. This effect is most pronounced for virgin materials after casting/heat treatment, but also affects their

service properties. Material scientists subsume such behaviour under the terminology *functional fatigue* [11–14] because of its detrimental effect on material reliability in technical applications.

Figure 1.9 (b) illustrates the situation of thermal hysteresis in the free energy/temperature diagram. Two transformation temperatures $T_{M \rightarrow A} > T_E$ and $T_{A \rightarrow M} < T_E$ are indicated along the abscissa. The two graphs in this figure represent the same equilibrium free energies of austenite and martensite, as in the reversible case of Fig. 1.9a. At $T_{M \rightarrow A} >$ and $T_{A \rightarrow M}$, the two graphs do not coincide but differ from one another by $\Delta f_B^{A \rightarrow M}$ and $\Delta f_B^{M \rightarrow A}$, respectively. These are interpreted as nucleation barriers. This suggests that in order to model hysteresis—the effects of undercooling and overheating with respect to T_E —the thermodynamic theory must be enriched by free energy nucleation barriers Δf_B .

According to the definition of the free energy such barriers consists of an energetic part Δu_B and an entropic part $T \Delta s_B$ in general,

$$\Delta f_B = \Delta u_B - T \Delta s_B. \quad (1.21)$$

For specific materials, the contributions of the energy and entropy to the free energy barrier may vary. In the classical nucleation theory of fluids, the free energy nucleation barrier is represented by tensional interface energy raised to establish phase boundaries [77]. This ansatz yields hysteresis in condensation/evaporation processes of fluids [78–80]. The classical work has motivated similar approaches for SMA. Here, interface energies are attributed to lattice mismatch of the respective phases, hence effecting potential strain energy along the interface. Solid–solid phase transformations are affected by *local* compatibility concerns and stress fields to either side of the interface [16, 18]. Interfacial strain energies are strongly orientation-dependent and affected by defects and dislocations. According to the classical crystallographic theory [52], martensitic twinning provides a mechanism to produce a strain-free habit plane on the macroscopic scale. On the microscopic length-scale however, some degree of lattice mismatch is inevitable, causing strain fields and local disconnections at the interface [81]. On average, these microscopic effects produce a interface energy and cause hysteretic phase diagrams. In turn, hysteresis should vanish in rare situations where the parent and the product lattices match perfectly even on the microscale. For example, if the second eigenvalue of the crystallographic transformation matrix, λ_2 , is equal to 1, the habit plane can be defined without a twinned martensite [82]: Perfectly match between parent and product is expected. Experimental studies seem to prove the relationship between $\lambda_2 \approx 1$ and small hysteresis [83].

Experiments give evidence hysteresis and functional fatigue in SMA indeed related to the microstructure developed during thermo-mechanical processes [86, 87]. The formation process has to account both for lattice mismatch between parent and product as well as between product variants which gives rise to specific interface energies. These interfere the transformation process by adding energetic nucleation barriers. Nucleations typically occur at loci where some pre-existing interfaces offer favourable conditions. They are influenced by stochastic fluctuations of the field vari-

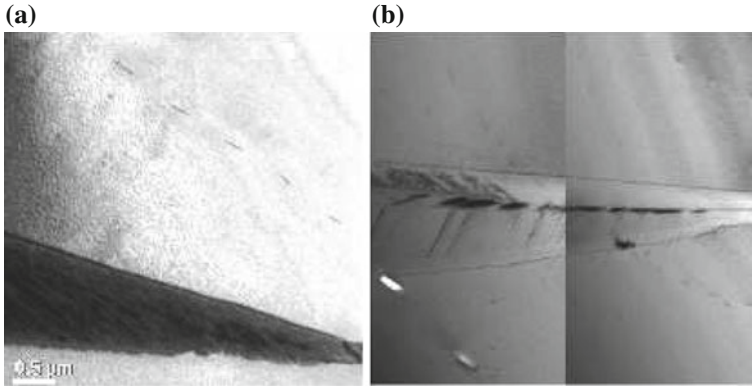


Fig. 1.10 TEM micrograph of the same region in a NiTi specimen upon temperature-induced martensitic transformation (a) and after the reverse transformation (b). The dark region in (a) indicates a T-induced martensite wedge. The wedge leaves faint dislocation marks in (b) after reverse transformation [84, 85] with courtesy of the authors

ables. Other experimental work reveals that the energetic situation at the interface between austenite and martensite is augmented by additional microstructural defects produced in both forward and reverse MT. The interaction of MT with any kind of structural defects (free surfaces, anti-phase boundaries, stacking faults, interfaces and precipitates) was intensely studied experimentally in recent years. An overview of the complexity of the physical situation is provided in [88] and applications have been made for CuZnAl [89] and AuCd [90]. The interactions of moving interfaces with such defects were investigated in [91] and [92] for Cu based alloys. The effect of aging on the temperature hysteresis in such alloys is documented in [93]. All these works refer to a strong relationship between the evolution of microstructural morphologies and the thermodynamic properties of the materials, indicating a history-dependence of the phase diagrams. Figure 1.10 illustrates a particular suggestive example of this: it shows the generation of a dislocative microstructure during forward and reverse MT in a NiTi sample. (a) and (b) show two TEM images of the same region within the sample during thermal forward MT in (a) and after completion of the reverse (b) [84, 85]. Note the wedge-shaped martensite region in (a) leaves behind a distinct dislocation footprint within the austenite matrix after reverse transformation faintly visible in (b). Thus, the forward/reverse transformation process has changed the lattice by adding new microstructural elements, dislocations in this case. Under cyclic thermal loading such microstructure develops and becomes more pronounced, see [94] for a study in Cu–Al–Mn. Sophisticated calorimetric studies unveil the influence of the temperature rates selected in an experiment [95] on thermal hysteresis.

Continuum models generally simplify solid–solid interfaces as singular surfaces (atomically sharp habit planes and twin boundaries) and assume phenomenological models for the surface energy. Typically, two approaches are taken [64]: either the interfaces are considered as singular surfaces with a localised surface energy [96],

or the interface is considered as a steep but smooth transition zone and the interface energy is modelled proportionally to the square of the strain gradient [58, 59].

Such nucleation barriers originate from mechanical effects and no entropic contributions to the nucleation barrier are regarded in these theories explicitly. However, for lattice transformations such effect must be expected. By MD simulations of nucleations events in 2D lattices we shall rationalise the nature of this entropic barrier (pages 97 ff).

1.3.3 Dynamics of Atomic Assemblies

The method of molecular dynamics is rooted in the concepts of classical mechanics. Here, the motions $\mathbf{x}_\alpha(t)$ of an assembly of $\alpha = 1, \dots, N$ atoms are calculated as functions of time on the basis of Newton's second law,

$$m_\alpha \ddot{\mathbf{x}}_\alpha = \mathbf{f}_\alpha \quad (\alpha = 1, \dots, N). \quad (1.22)$$

Atoms are mathematically considered as points with masses m_α . The Equations of Motion (1.22) represent a set of second-order differential equations. Their integration therefore involves two constants of integration per atom to be determined from initial conditions.

The forces \mathbf{f}_α have two additive contributions: internal forces $\mathbf{f}_\alpha^{\text{int}}$ and external forces $\mathbf{f}_\alpha^{\text{ext}}$

$$\mathbf{f}_\alpha = \mathbf{f}_\alpha^{\text{int}} + \mathbf{f}_\alpha^{\text{ext}}. \quad (1.23)$$

Internal forces arise from the atomic interactions, while external forces result from external force fields, such as gravitation, electrical and magnetic fields and from constraints acting on the surface of the assembly.

Internal and external forces may be represented as gradient fields of the internal and external potential functions $V^{\text{int}}(\mathbf{x}_\gamma)$ and $V^{\text{ext}}(\mathbf{x}_\gamma, t)$, respectively:

$$\mathbf{f}_\alpha^{\text{int}} = -\nabla_\alpha V^{\text{int}}(\mathbf{x}_\gamma), \quad (1.24)$$

$$\mathbf{f}_\alpha^{\text{ext}} = -\nabla_\alpha V^{\text{ext}}(\mathbf{x}_\gamma, t). \quad (1.25)$$

The internal potential V^{int} is a material property and depends on the positions of all $\gamma = 1, \dots, N$ atoms. This quantity does not depend explicitly on time t but only implicitly through the time dependency of the atomic positions. In contrast to this, the external potential V^{ext} may also depend explicitly on t , as required by the external force fields.

The atomic velocities are obtained by differentiation of the motions with respect to time, $\dot{\mathbf{x}}_\alpha$. The centre of mass \mathbf{x} of the total assembly, the velocity of this mass centre \mathbf{v} and the excess atomic velocities \mathbf{c}_α are defined by

$$\mathbf{x} = \sum_{\alpha=1} \frac{m_{\alpha}}{m} \mathbf{x}_{\alpha}, \quad (1.26)$$

$$\mathbf{v} = \sum_{\alpha=1} \frac{m_{\alpha}}{m} \dot{\mathbf{x}}_{\alpha}, \quad (1.27)$$

$$\mathbf{c}_{\alpha} = \dot{\mathbf{x}}_{\alpha} - \mathbf{v}. \quad (1.28)$$

Here, $m = \sum_{\alpha} m_{\alpha}$ is the total mass. Note that the N individual excess velocities \mathbf{c}_{α} are not entirely independent of each other, since the relation $\sum_{\alpha} m_{\alpha} \mathbf{c}_{\alpha} = 0$ holds true.

Regarding the Eqs. (1.23)–(1.26), summation of Newton’s second law (1.22) over α yields Newton’s first law, the Momentum Equation,

$$m\mathbf{v} = \sum_{\alpha=1}^N \mathbf{f}_{\alpha}^{\text{ext}}. \quad (1.29)$$

This equation states that the momentum of the mass centre ($m\mathbf{v}$) is conserved in the absence of external forces.

The energy equation for the atomic assembly is obtained by a scalar-multiplication of Eq. (1.22) by $\dot{\mathbf{x}}_{\alpha}$ and subsequently summing over N . The result may be rewritten in the popular form by using Eqs. (1.24)–(1.28),

$$\frac{d}{dt} \left(\frac{m}{2} v^2 + V^{\text{ext}}(\mathbf{x}_{\gamma}, t) + V^{\text{int}}(\mathbf{x}_{\gamma}) + \sum_{\alpha=1}^N \frac{m_{\alpha}}{2} c_{\alpha}^2 \right) = \frac{\partial V^{\text{ext}}}{\partial t}. \quad (1.30)$$

Consequently, if the external potential V^{ext} does not change with time, the quantity within the parenthesis—the total energy \mathcal{E} of the system—is conserved:

$$\frac{\partial V^{\text{ext}}}{\partial t} = 0 \quad \Rightarrow \quad \frac{m}{2} v^2 + V^{\text{ext}}(\mathbf{x}_{\gamma}, t) + V^{\text{int}}(\mathbf{x}_{\gamma}) + \underbrace{\sum_{\alpha=1}^N \frac{m_{\alpha}}{2} c_{\alpha}^2}_{\mathcal{E}} = \mathcal{E} = \text{const}. \quad (1.31)$$

The total energy \mathcal{E} consists of three parts: the (macroscopic) kinetic energy K , which is related to the square of the velocity of the mass centre, the potential energy of external force fields and the term underlined in Eq. (1.31). This term models the internal energy U of the assembly. It originates from the atomic interaction potential and from the kinetic excess energy.

We may also introduce the Lagrangian mechanics briefly since it is frequently used in the MD-related literature. Lagrange’s approach is convenient in situations where the atomic motions need to be represented in non-Cartesian coordinates, or if special constraints need to be incorporated in the formulation. Lagrange considered the equation

$$\sum_{\alpha=1}^n (m_{\alpha} \ddot{\mathbf{x}}_{\alpha} - \mathbf{f}_{\alpha}) d\mathbf{x}_{\alpha} = 0, \quad (1.32)$$

which represents an alternative formulation of Newton's equations of motion (1.22), and applied a bijective variable transformation of the type

$$q_k = q_k(\mathbf{x}_{\alpha}, t) \quad (k = 1, \dots, 3N) \quad \Leftrightarrow \quad \mathbf{x}_{\alpha} = \mathbf{x}_{\alpha}(q_1, \dots, q_{3N}, t). \quad (1.33)$$

In the case of an *unconstrained* system, i.e. a system not subject to any external force field, an application of the transformation (1.33) in (1.32) yields a new set of $3N$ differential equations which control the motions of the atoms. These are called Lagrange's equation of motion,

$$\frac{d}{dt} \left(\frac{\partial \mathcal{L}}{\partial \dot{q}_k} \right) = \frac{\partial \mathcal{L}}{\partial q_k}. \quad (1.34)$$

\dot{q}_k , as usual, denote the time-derivatives of the coordinates q_k and \mathcal{L} is called the *Langrangian*, an energy function representing the difference of the kinetic energy $T(\dot{q}_k)$ and potential energy $V^{\text{int}}(q_k)$ of the unconstrained system,

$$\mathcal{L} = T(\dot{q}_k) - V^{\text{int}}(q_k). \quad (1.35)$$

Lagrange's and Newton's equations of motion (1.22), (1.34) are identical if the coordinates q_k are represented in a Cartesian frame. In this case the Lagrangian reads

$$\mathcal{L}(\mathbf{x}_{\alpha}, \dot{\mathbf{x}}_{\alpha}) = \sum_{\alpha=1}^N \frac{m_{\alpha}}{2} \dot{\mathbf{x}}_{\alpha}^2 - V^{\text{int}}(\mathbf{x}_{\alpha}). \quad (1.36)$$

Up to this point, the model's equations rest entirely on the axioms of Newton, which represent first principles of physics. To calculate the atomic motions for a specific material we need to define the potential V^{int} as functions of the atomic positions.

1.3.4 Statistical Thermodynamics

The macroscopic energy state of an N -atom assembly is entirely determined by the atomic micro-states $\{\mathbf{x}_{\alpha}(t), \dot{\mathbf{x}}_{\alpha}(t)\}$. This $6N$ -tuple indicates a *phase* of the assembly. It may be represented by a point in the $6N$ -dimensional phase space, in which it moves along a trajectory as a function of time. If the assembly is unconstrained, the energy state is entirely determined by the initial phase $\{\mathbf{x}_{\alpha}(t_0), \dot{\mathbf{x}}_{\alpha}(t_0)\}$ at the initial time t_0 owing to Eq. (1.31). Thus, the trajectory of the unconstrained assembly is bound to a hyperplane of the phase space determined by the initial energy $\mathcal{E}(t_0)$, which is

constant. Since we are dealing with a classical system, this trajectory represents a continuous line, parametric in time. Along this line, ν observations of the assembly at consecutive times (t_1, \dots, t_ν) yield an ensemble of phases, all indicated by the same total energy. Such an ensemble is called a “microcanonical” ensemble of phases.

A subset of S atoms of the N -atom assembly has the energy $\mathcal{E}^S(\mathbf{x}^1, \dot{\mathbf{x}}^1, \dots, \mathbf{x}^S, \dot{\mathbf{x}}^S)$. This energy is variable, since the S atoms thermally interact with the $N - S$ residual atoms in the assembly. Thus, the residual assembly constitutes an environment of the subset. Among ν consecutive observations of the subset, we see the given phases $\{\mathbf{x}^1, \dot{\mathbf{x}}^1, \dots, \mathbf{x}^S, \dot{\mathbf{x}}^S\}$ μ times. Therefore, if ν is big enough, the probability of observing this phase is

$$P(\mathbf{x}^1, \dot{\mathbf{x}}^1, \dots, \mathbf{x}^S, \dot{\mathbf{x}}^S) = \frac{\mu(\mathbf{x}^1, \dot{\mathbf{x}}^1, \dots, \mathbf{x}^S, \dot{\mathbf{x}}^S)}{\nu}. \quad (1.37)$$

By using the arguments of statistical thermodynamics, the probability of seeing the subset in the phases $\{\mathbf{x}^1, \dot{\mathbf{x}}^1, \dots, \mathbf{x}^S, \dot{\mathbf{x}}^S\}$ can be expressed in terms of the energy of the subset and T ,

$$P(\mathbf{x}^1, \dot{\mathbf{x}}^1, \dots, \mathbf{x}^S, \dot{\mathbf{x}}^S) = \frac{\exp\left(-\frac{\mathcal{E}^S(\mathbf{x}^1, \dots, \mathbf{x}^S)}{kT}\right)}{\sum_{\mathbf{x}^1} \sum_{\dot{\mathbf{x}}^1} \dots \sum_{\mathbf{x}^S} \sum_{\dot{\mathbf{x}}^S} \exp\left(-\frac{\mathcal{E}^S(\mathbf{x}^1, \dots, \mathbf{x}^S)}{kT}\right)}. \quad (1.38)$$

This is the “canonical” probability distribution. It is a function of the positions and velocities of the particles belonging exclusively to the subset. The $N - S$ residual particles contribute only to the temperature of the subset, because the subset S of N atoms shares the mean kinetic energy with the residual system of $N - S$ atoms. Therefore, the residual body may be interpreted as a heat bath, which provides a constant temperature for the subset. The concept of microcanonical ensembles and their related subsystems originates from Maxwell and his contemporary Boltzmann. The factor $1/kT$ was identified by applying the concept to monatomic, ideal gases.

The concepts of Maxwell and Boltzmann were generalised by Gibbs from the special situation of “subsets within larger systems” to generic ensembles of systems. Instead of considering an ensemble of ν consecutive observations, Gibbs—in a leap of imagination—suggested an ensemble of ν replicas of one system. These replicas are supposed to “weakly interact” in order to allow them to exchange energy. The total energy of this ensemble of replicas and the ensemble size ν are supposed to be constant. Hence, all ν replicas collectively establish the energetic environment for an individual ensemble member. This metaphorically replaces the overall atomic assembly at constant energy considered by Maxwell and Boltzmann. Consequently, the studied replicas may be of arbitrary size. The assumption that the time average of a system’s observable equals the ensemble average of this observable in a system of replicas is known as the ergodic hypothesis.

We may abbreviate the energy states of an individual replica in Gibbs' ensemble by \mathcal{E}_l and denote the number of replicas which are found to occupy this state by μ_l . This energy state is a single and discrete state of $1, \dots, M$ energy states which are invariably available to the replica. Hence, the number series μ_l represents a distribution of replicas over these energy states, such that $\sum_{l=1}^M \mu_l = v$. Gibbs employed Boltzmann's formula for the ensemble's entropy, $\mathcal{S} = k \log W$ with

$$W = \frac{v!}{\prod_{l=1}^M \mu_l!}, \quad (1.39)$$

in order to calculate the equilibrium distribution of $\mu_l|_E$ by maximising the entropy subject to the constraints of constant energy $\mathcal{E} = \sum \mu_l \mathcal{E}_l$ and constant v . This procedure yields a canonical distribution of energy states:

$$P_l = \left(\frac{\mu_l|_E}{v} \right) = \frac{\exp\left(-\frac{\mathcal{E}_l}{kT}\right)}{\sum_{l=1}^M \exp\left(-\frac{\mathcal{E}_l}{kT}\right)}. \quad (1.40)$$

The suffix "E" again indicates that the result refers to thermodynamic equilibrium. Note the factor $1/kT$ enters Eq. (1.40) via the energy constraint during the maximisation computation.

If we interpret \mathcal{E}_l as a short form for the energy state $\mathcal{E}^S(\mathbf{x}_1 \dots \mathbf{x}_S)$ of Maxwell's subset ensemble, the results of Eqs. (1.40) and (1.38) are identical, although they have been derived differently. Gibbs' result, however, is more general because it applies to any ensemble at constant temperature regardless of how these isothermal conditions are maintained. Equation (1.40) may be used to calculate the expectation value of energy of an individual replica in the ensemble, $\langle \mathcal{E} \rangle$, and the expectation value of entropy, $\langle \mathcal{S} \rangle$:

$$\langle \mathcal{E} \rangle = \left. \frac{\mathcal{E}}{v} \right|_E = kT^2 \frac{\partial \log Z}{\partial T}, \quad (1.41)$$

$$\langle \mathcal{S} \rangle = \left. \frac{\mathcal{S}}{v} \right|_E = \frac{\langle \mathcal{E} \rangle}{T} + k \log Z. \quad (1.42)$$

In these two equations, Z denotes an abbreviation for the denominator of (1.40), called the canonical partition function.

We may now consider an N -atom ensemble at constant T , irrespective of how this temperature is maintained. The partition function of such a system is given by

$$Z = \sum_{\mathbf{x}_1, \dots, \mathbf{x}_N} \sum_{\dot{\mathbf{x}}_1, \dots, \dot{\mathbf{x}}_N} \exp \left(- \frac{\frac{m}{2} v^2 + V^{\text{int}}(\mathbf{x}_\gamma) + \sum_{\alpha=1}^N \frac{m_\alpha}{2} (\dot{\mathbf{x}}_\alpha - \mathbf{v})^2}{kT} \right). \quad (1.43)$$

This function cannot, in general, be analytically calculated because the interaction potential is a complicated function of the atomic positions. However, an analytical result exists for crystals subject to two restrictive assumptions:

1. Einstein crystal: Atoms are considered to move independently of one another within mean potential energy functions V_α^{int} provided by their average environment,

$$V^{\text{int}} = \sum_{\alpha=1}^N V_\alpha^{\text{int}}(\mathbf{x}_\alpha) \quad (1.44)$$

2. Harmonic approximation: The atoms are considered as harmonic oscillators, such that the mean potential energy of an individual atom may be represented by a quadratic function:

$$V_\alpha^{\text{int}}(\mathbf{x}_\alpha) = \frac{\lambda_\alpha}{2} (\mathbf{x}_\alpha - \mathbf{X}_\alpha^0)^2 + e_\alpha^0. \quad (1.45)$$

In Eq. (1.45), the λ_α denote the curvatures of the parabolic mean potential energies of atoms vibrating about the ground-state positions \mathbf{X}_α^0 . Note that the second assumption excludes any anisotropy of the potential as well as thermal expansion. $e_\alpha^0 = V_\alpha^{\text{int}}(\mathbf{X}_\alpha^0)$ represents the ground-state energy at $T \rightarrow 0$. Regarding these assumptions, Eq. (1.43) can be analytically computed. For this purpose we approximate sums by integrals and obtain

$$\begin{aligned} Z &\approx \exp\left(-\frac{mv^2}{2kt}\right) \cdot \prod_{\alpha=1}^N \frac{1}{Y} \int_{-\infty}^{\infty} \exp\left(-\frac{m_\alpha(\dot{\mathbf{x}}_\alpha - \mathbf{v})^2 + \lambda_\alpha(\mathbf{x}_\alpha - \mathbf{X}_\alpha^0)^2 + 2e_\alpha^0}{2kT}\right) dx_1 \dots d\dot{x}_N \\ &= \exp\left(-\frac{mv^2}{2kT}\right) \exp\left(-\sum_{\alpha=1}^N \frac{e_\alpha^0}{kT}\right) \frac{1}{Y} \prod_{\alpha=1}^N \frac{(2\pi kT)^3}{\sqrt{\lambda_\alpha m_\alpha}^3}. \end{aligned} \quad (1.46)$$

Y is a constant factor that attends to the correct discretisation of the phase space when switching from the quantised to the continuous representation. With this result, the expectation of the energy (1.41) reads

$$\langle \mathcal{E} \rangle = \underbrace{\frac{m}{2} v^2}_K + \underbrace{3NkT + \sum_{\alpha=1}^n e_\alpha^0}_U. \quad (1.47)$$

This energy consists of two parts, the kinetic energy K of the mass centre of the total ensemble and the internal energy U . It is instructive to decompose U into the two parts of Eq. (1.48), representing the expectation value of the kinetic excess energy

$\langle \mathcal{E}_{\text{kin}}^{\text{excess}} \rangle = \sum m_\alpha / 2 c_\alpha^2$, and the expectation value of the internal potential energy $\langle V^{\text{int}} \rangle$,

$$U = \underbrace{\frac{3}{2} NkT}_{\langle \mathcal{E}_{\text{kin}}^{\text{excess}} \rangle} + \underbrace{\sum_{\alpha=1}^N e_\alpha^0 + \frac{3}{2} NkT}_{\langle V^{\text{int}} \rangle}. \quad (1.48)$$

We see at mean, the internal potential energy of a vibrating atom assembly is T -dependent. Further, the temperature is proportional to the mean kinetic energy of the excess velocities $\mathbf{c}_\alpha = \dot{\mathbf{x}}_\alpha - \mathbf{v}$, while the velocity of the mass centre \mathbf{v} does not contribute to temperature.

The expectation value of the equilibrium entropy S is given by

$$S = \langle \mathcal{S} \rangle = \frac{3}{2} Nk \log(kT) + k \sum_{\alpha=1}^N \log \left\{ \frac{4}{3} \pi \sqrt{\frac{3kT}{\lambda_\alpha}}^3 \right\} + \underbrace{3Nk + k \log \left\{ \frac{1}{Y} \prod_{\alpha=1}^N \left(\frac{2\pi^2}{3m_\alpha^{\frac{3}{2}}} \right) \right\}}_{=C} \quad (1.49)$$

This entropy is composed of three terms. The last term in Eq. (1.49) represents the entropy constant denoted by C . The first term represents the usual caloric part which is identical for monatomic ideal gases. The underlined term in Eq. (1.49) results from the potential energy V^{int} . This term needs to be interpreted: According to the rules of statistics, $\sqrt{3kT/\lambda_\alpha}$ represents the mean amplitude (standard deviation) of the atomic oscillations about the ground state positions at a given temperature T . The magnitude of this amplitude is controlled by T and by the curvature λ_α of the potential, see Eq. (1.45): At a given T , broader potentials (characterised by “small” λ) allow larger amplitudes than narrower potentials (characterised by “large” λ). Hence, the logarithm’s argument in the underlined term of Eq. (1.49) may be geometrically interpreted as the spherical volume available to an atom corresponding to this amplitude. It represents a measure of the atomic mobility in a quadratic potential. The larger this volume, the more microstates an individual atom may occupy in phase space and consequently, the higher the entropy. We shall return to this discussion in Chap.3 when evaluating the entropies of austenitic and martensitic lattices.

Finally, according to the harmonic potential model, the expectation of the free energy $F = U - TS$, results from a combination of internal energy and entropy,

$$F = 3NkT + \sum_{\alpha=1}^N e_\alpha^0 - \frac{3}{2} NkT \log(kT) - kT \sum_{\alpha=1}^N \log \left\{ \frac{4}{3} \pi \sqrt{\frac{3kT}{\lambda_\alpha}}^3 \right\} - TC. \quad (1.50)$$

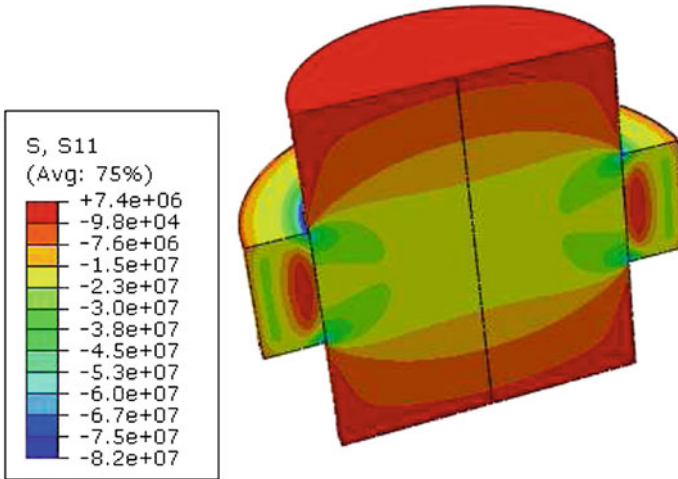


Fig. 1.11 Shrink-fit FEM simulation of a SMA bush onto a Hookean shaft during heating. The bush is radially pre-strained in the martensite phase (low T) so as to become pseudo-plastically deformed. Next, it is placed on the shaft and heated, thus triggering the SME. Contraction fixes the bush and visibly affects the radial stress distribution shown. The figure shows an axial cross-section of shaft and bush in the final state [97]

1.4 Engineering Models of SMA

For design studies of engineering applications it is often not necessary to model the full microscopic complexity of SMA. Rather, models must be reliably capable of the thermo-mechanical coupling: pseudo-plasticity, pseudo-elasticity, the shape memory effect and latent heat effects. Other requirements include their practical use in numerical algorithms such as FEM platforms, their numerical precision, robustness and efficiency.

Models developed for this purpose may be roughly divided into three groups: empirical models, plasticity models and energy-based models. Early empirical models use suitable ansatz functions, fitted to measurements in the state space. Such models are, however, only reliable within their circumscribed boundaries. Models are partly restricted to pseudo-elasticity [98–100]. More sophisticated models introduce internal variables to incorporate one- or two-way effects [101]. Another group of models are rooted in the classical theory of plasticity [102–105]. Physically more sophisticated models are based on free-energy descriptions of the material [106–109]. Temperature changes caused by latent transformation heats are an integral part of the behaviour of shape memory alloys and inevitably couple the thermal and the mechanical fields. This general behaviour is fully covered by the Müller–Achenbach–Seelecke (MAS) model. First published in 1979 [110], the MAS model has been explored and improved over the years. Important contributions were due to Achenbach [111] and Seelecke [112, 113]. At the Department of Materials Science

at the Ruhr-University Bochum, a research group is dealing with the implementation of this model into the FEM platform ABAQUSTM. Originally, the MAS model is restricted to uni-axial states of stress, which limits its application to cases where only these stress states prevail, such as axial loading in wires and trusses, pure beam bending, pure torsion and shrink-fit problems as well as thermally-induced processes in absence of external loading. These problems have already been studied by FEM [97, 114–117], see Fig. 1.11 for an example. To overcome this uni-axial limitation, the model has been extended to arbitrary 3D stress/strain/temperature states [118, 119].

References

1. L.C. Chang, T.A. Read, Plastic deformation and diffusionless phase changes in metals – the gold-cadmium beta phase. *Trans. AIME* **189**(1), 47–52 (1951)
2. W.J. Buehler, R.C. Wiley, J.W. Gilfrich, Effect of low-temperature phase changes on mechanical properties of alloys near composition TiNi. *J. Appl. Phys.* **34**(5), 1475 (1963)
3. R.J. Wasilews, S.R. Butler, J.E. Hanlon, Martensitic transformation in TiNi. *J. Metals* **17**(9), 1965 (1965)
4. M.W. Burkart, T.A. Read, Diffusionless phase change in the indium-thallium system. *Trans. AIME* **197**(11), 1516–1524 (1953)
5. E. Hornbogen, G. Wassermann, Über den Einfluß von Spannungen und das Auftreten von Umwandlungsplastizität bei der $\beta_1 - \beta''$ -Umwandlung des Messing. *Z. Metallkd.* **47**(6), 427–433 (1956)
6. E. Hornbogen, A. Segmüller, G. Wassermann, Martensitische Umwandlung bei der Verformung von abgeschrecktem beta-1-Messing. *Z. Metallkd.* **48**(7), 379–384 (1957)
7. H. Pops, T.B. Massalski, Thermoelastic + burst-type martensites in copper-zinc beta-phase alloys. *Trans. AIME* **230**(7), 1662 (1964)
8. C.W. Chen, Some characteristic quantities of the martensite transformation of Cu-Al-Ni alloys. *Trans. AIME* **209**, 1202–1203 (1957)
9. A. Musolff, Load-strain-temperature measurements of a NiTi wire. Department of Thermodynamics, Technical University of Berlin. Personally communicated (2003)
10. M. Wagner, J. Frenzel, Cyclic experiments with a NiTi wire. Department of Materials Science, Ruhr-University Bochum. Personally communicated (2008)
11. E. Hornbogen, Thermo-mechanical fatigue of shape memory alloys. *J. Mater. Sci.* **38**, 1–15 (2003)
12. G. Eggeler, E. Hornbogen, A. Yawny, A. Heckmann, M. Wagner, Structural and functional fatigue of NiTi shape memory alloys. *Mater. Sci. Eng. A* **378**, 24–33 (2004)
13. E. Hornbogen, Shape memory alloys, in *Advanced Structural and Functional Materials*, ed. by G.J. Bunk (Springer, Heidelberg, 1991), pp. 133–163
14. E. Hornbogen, G. Eggeler, Surface aspects and fatigue of shape memory alloys (SMAs). *Mat.-wiss. u. Werkstofftech.* **34**, 255–259 (2004)
15. K. Otsuka, C.M. Wayman, (eds.) *Shape Memory Materials* (Cambridge University Press, Cambridge, 1998)
16. J.W. Christian, *The theory of transformations in metals and alloys, volume I, II* (Pergamon, Amsterdam, 2002)
17. K. Otsuka, C.M. Wayman, K. Nakai, Superelasticity effects and stress-induced martensitic transformations in Cu-Al-Ni alloys. *Acta Metall.* **24**(3), 207–226 (1976)
18. K. Bhattacharya, *Microstructure of Martensite—Why it Forms and How it Gives Rise to the Shape-Memory Effect*. (Oxford University Press, Oxford, 2003)

19. J. Philibert, Cinétique de la transformation martensitique dans und ferronickel. Comptes rendus hebdomadaires des séances de l'Académie des Sciences **240**(5), 529–531 (1955)
20. R.C. O'Handley, Model for strain and magnetization in magnetic shape-memory alloys. Journal Appl. Phys. **83**(6), 3263–3270 (1998)
21. A.N. Vasil'ev, A.D. Bozhko, V.V. Khovailo, I.E. Dikshtein, V.G. Shavrov, V.D. Buchelnikov, M. Matsumoto, S. Suzuki, T. Takagi, J. Tani, Structural and magnetic phase transitions in shape-memory alloys $\text{Ni}_{2+x}\text{Mn}_{1-x}\text{Ga}$. Phys. Rev. B **59**(2), 1113–1120 (1999)
22. K. Oikawa, L. Wulff, T. Iijima, F. Gejima, T. Ohmori, A. Fujita, K. Fukamichi, R. Kainuma, K. Ishida, Promising ferromagnetic Ni-Co-Al shape memory alloy system. Appl. Phys. Lett. **79**(20), 3290–3292 (2001)
23. P.W. Anderson, E.I. Blount, Symmetry considerations on martensitic transformations - ferroelectric metals. Phys. Rev. Lett. **14**(7), 217 (1965)
24. K. Otsuka, X. Ren, Physical metallurgy of Ti-Ni-based shape memory alloys. Prog. Mat. Sci. **50**(5), 511–678 (2005)
25. T.H. Nam, T. Saburi, K. Shimizu, Cu-content dependence of shape memory characteristics in Ti-Ni-Cu alloys. Mat. Trans. JIM **31**(11), 959–967 (1990)
26. J.D. Busch, A.D. Johnson, C.H. Lee, D.A. Stevenson, Shape-memory properties in Ni-Ti sputter-deposited film. J. Appl. Physics **68**(12), 6224–6228 (1990)
27. O. Matsumoto, S. Miyazaki, K. Otsuka, H. Tamura, Crystallography of martensitic-transformation in Ti-Ni single-crystals. Acta Metall. **35**(8), 2137–2144 (1987)
28. S. Miyazaki, K. Otsuka, C.M. Wayman, The shape memory mechanism associated with the martensitic-transformation in Ti-Ni alloys. 1. self-accommodation. Acta Metall. **37**(7), 1873–1884 (1989)
29. K. Otsuka, C.M. Wayman, K. Nakai, H. Sakamoto, K. Shimizu, Superelasticity effects and stress-induced martensitic transformations in Cu-Al-Ni alloys. Acta Metall. **24**(3), 207–226 (1976)
30. K. Otsuka, H. Sakamoto, K. Shimizu, Successive stress-induced martensitic transformations and associated transformation pseudoelasticity in Cu-Al-Ni alloys. Acta Metall. **27**(4), 585–601 (1979)
31. K.E. Easterli, H.M. Miekkoja, Martensitic transformation of iron precipitates in a copper matrix. Acta Metall. **15**(7), 1133 (1967)
32. J. Perkins, R.O. Sponholz, Stress-induced martensitic-transformation cycling and 2-way shape memory training in Cu-ZnAl alloys. Metall. Trans. A Phys. Metall. Mat. Sci. **15**(2), 313–321 (1984)
33. K. Otsuka, K. Shimizu, Memory effect and thermoelastic martensite transformation in Cu-Al-Ni alloy. Scripta Metall. **4**(6), 469 (1970)
34. Z.-Z. Yu, P.C. Clapp, Growth dynamics study of the martensitic transformation in Fe-30 pct Ni alloys: Part II. computer simulation of martensitic growth. Metall. Trans. A **20A**, 1617–1629 (1989)
35. K.Y. Lee, J.R. Ray, Mechanism of pressure-induced martensitic phase-transformations - a molecular-dynamics study. Phys. Rev. B **39**(1), 565–574 (1989)
36. P.C. Clapp, J. Rifkin, Nucleation of a martensite in a computer. in Proceedings of International Conference on Solid-Solid Phase Transformations, (TMS-AIME, Warrendale, 1982), pp. 1165–1169
37. R. Meyer, P. Entel, Martensite-austenite transition and phonon dispersion curves of $\text{Fe}_{1-x}\text{Ni}_x$ studied by molecular-dynamic simulations. Phys. Rev. B **57**(9), 5140–5147 (1998)
38. S. Rubini, P. Ballone, Quasi-harmonic and molecular-dynamics study of the martensitic-transformation in Ni-Al alloys. Phys. Rev. B **48**(1), 99–111 (1993)
39. W.W. Liang, M. Zhou, Atomistic simulations reveal shape memory of fcc metal nanowires. Phys. Rev. B **73**(11) (2006)
40. U. Pinsook, G.J. Ackland, Atomistic simulation of shear in a martensitic twinned microstructure. Phys. Rev. B **62**(9), 5427–5434 (2000)
41. Institute for Scientific Information. Web of science. Internet database, <http://portal.isiknowledge.com>

42. P.C. Clapp, How would we recognise a martensitic transformation if it bumped into us on a dark & austy night? in Proceedings of the International Conference On Martensitic Transformations, ed. by R. Gotthard, J. Van Humbeeck, vol I of Les Editions de Physique, (Lausanne, Switzerland, 1995), pp. C8–11–C8–19
43. G.B. Olson, W.S. Owen, *Martensite* (The Materials Information Society, ASM international, 1992)
44. S. Tan, H. Xu, Observations on a CuAlNi single crystall. Continuum Mech. Therm. **2**, 241–244 (1990)
45. A. Schäfer, O. Kastner, DSI observation of temperature-induced martensitic transformtions in a CuNiAl single crytal plate. (Department of Material Science, Ruhr-University Bochum, Germany, 2010)
46. Ch. Somsen, TEM observations in NiTi and NiTiFe. Department of Materials Science, Ruhr-University Bochum. Personally communicated (2010)
47. T. Waitz, The self accomodated morphology of martensite in nanocrystalline NiTi shape memory alloys. Acta Mater. **53**(8), 2273–2283 (2005)
48. P. Boullay, D. Schryvers, J.M. Ball, Nano-structures at martensite macro twin interfaces in Ni₆₅Al₃₅. Acta Mater. **51**(5), 1421–1436 (2003)
49. A.-L. Cauchy, Sur l'Equilibre et le Mouvement d'un Systeme de Points Materiels. in Oeuvres Completes d'Augustin Cauchy, number 8 in 2, (1890), pp. 227–252
50. M. Born, *Dynamik der Kristallgitter*. (Teubner, 1915)
51. I. Müller, *A History of Thermodynamics*. (Springer, Berlin, 2007)
52. M.S. Wechsler, D.S. Lieberman, T.A. Read, On the theory of the formation of martensite. Trans. AIME **197**(11), 1503–1515 (1953)
53. J.S. Bowles, J.K. Mackenzie, The crystallography of martensite transformations i. Acta Metall. **2**, 129–137 (1954)
54. J.S. Bowles, J.K. Mackenzie, The crystallography of martensite transformations ii. Acta Metall. **2**, 138–147 (1954)
55. C.M. Wayman, *Introduction to the Crystallography of Martensitic Transformations* (The MacMillan Company, New York, 1964)
56. H. Schumann, *Kristallgeometrie* (Einführung in die Theorie der Gittertransformationen metallischer Werkstoffe. VEB Deutscher Verlag für Grundstoffforschung, Leipzig, 1979)
57. J.M. Ball, R.D. James, Fine phase mixtures as minimizers of energy. Archive for Rational Mechanics And Analysis **100**(1), 13–52 (1987)
58. J.D. van der Waals, The thermodynamic theory of capillarity under the hypothesis of a continuous variation of density. J. Stat. Phys. **20**(2), 200–244 (1979) Translation of the original work from 1893
59. J.W. Cahn, J.E. Hilliard, Free energy of a nonuniform system, I. interfacial free energy. J. Chem. Phys. **28**, 258–267 (1958)
60. J. Carr, M.E. Gurtin, M. Slemrod, Structured phase transition on a finite interval. Arch. Rat. Mech. Anal. **86**, 317–351 (1984)
61. L. Modica, Gradient theory of phase transitions and minimal interface criteria. Arch. Rat. Mech. Anal. **98**(2), 132–142 (1987)
62. I. Fonseca, The gradient theory of phase transitions for systems with two potential wells. Proc. R. Soc. Edinb. **111A**, 89–102 (1989)
63. L. Truskinovsky, G. Zanzotto, Finite-scale microstructures and metastability in one-dimensional elasticity. Meccanica **30**, 577–589 (1995)
64. Y. Huo, I. Müller, Interfacial and inhomogeneity penalties in phase transitions. Continuum Mech. Therm. **15**, 395–407 (2003)
65. A.G. Khachaturyan, *Theory of Structural Transformations in Solids*. (John Wiley & Sons, New York, 1983)
66. Y. Wang, A.G. Khachaturyan, Three-dimensional field model and computer modeling of martensitic transformations. Acta Mater. **45**(2), 759–773 (1997)
67. R. Abeyaratne, J.K. Knowles, Kinetic relations and the propagation of phase boundaries in solids. Arch. Rat. Mech. Anal. **114**, 119–154 (1991)

68. R. Abeyaratne, J.K. Knowles, Dynamics of propagating phase boundaries: Thermoelastic solids with heat conduction. *Arch. Rat. Mech. Anal.* **126**, 203–230 (1994)
69. L.M. Truskinovsky, Dynamics of non-equilibrium phase boundaries in a heat conducting non-linearly elastic medium. *J. Appl. Math. Mech. (PMM)* **53**, 777–784 (1987)
70. I. Müller, *Thermodynamics*. (Pitman Advanced Publishing Program, Pitman, Bosten, 1985)
71. I. Müller, W.H. Müller, *Fundamentals of Thermodynamics and Applications: With Historical Annotations and Many Citations from Avogadro to Zermelo*. (Springer, Berlin, 2009)
72. I. Müller, *Lectures on Statistical Mechanics, Parts I and II*. (Johns Hopkins University, Baltimore, 1974) Lecture Script
73. C. Truesdell, *Lectures on Rational Mechanics. Statistical Mechanics*. (Johns Hopkins University, Baltimore) Lecture Script
74. E. Schroedinger, *Statistische Thermodynamik* (Johann Ambrosius Barth, Leipzig, 1952)
75. I. Müller, W. Weiss, *Entropy and Energy*. (Springer, Berlin, 2005)
76. L.D. Landau, E.M. Lifshitz, *Theory of Elasticity*, vol 7, Course of Theoretical Physics. 3 edn (Elsevier, Amsterdam, 1986)
77. W. Thomson, On the equilibrium of vapour at a curved surface of liquid. *Proc. Roy. Soc. Edinburgh* **7**, (1872)
78. I. Müller, Boiling and condensation with interfacial energy. *Meccanica* **31**, (1996)
79. Y. Huo, I. Müller, Nucleation of droplets in a binary mixture. *Meccanica* **38**, 493–504 (2003)
80. J. Ansorg, I. Müller, Phase diagrams—heat of mixing and interfacial energy. In *Solid Mechanics and its Applications*, ed. by P. Argoul, M. Fremond, Q.S. Nguyen, IUMTAM Symposium on Variations of Domains and Free-Boundary Problems in Solid Mechanics. (Kluwer Academic Press, Dordrecht, 1999)
81. R.C. Pond, S. Celotto, J.P. Hirth, A comparison of the phenomenological theory of martensitic transformations with a model based on interfacial defects. *Acta Mater.* **51**, 5385–5398 (2003)
82. Z. Zhang, R.D. James, S. Müller, Energy barriers and hysteresis in martensitic phase transformations. *Acta Mater.* **57**, 4332–4352 (2009)
83. J. Cui, Y. Chu, O.O. Famodu, Y. Furuya, J. Hattrick-Simpers, R.D. James, A. Ludwig, S. Thienhaus, M. Wuttig, Z. Zhang, I. Takeuchi, Combinatorial search of thermoelastic shape memory alloys with extremely small hysteresis width. *Nature Mat.* **5**, 286–290 (2006)
84. T. Simon, A. Kröger, A. Dlouhy, G. Eggeler. In-situ tem cooling/heating experiments on deformed NiTi shape memory single crystals. in ESOMAT 2009. EDP Sciences (2009)
85. T. Simon, A. Kröger, A. Dlouhy, G. Eggeler, On the multiplication of dislocations during martensitic transformations in NiTi shape memory alloys. *Acta Mater.* **58**(5), 1850–1860 (2010)
86. H. Sitepu, W.W. Schmahl, J. Khalil-Allafi, G. Eggeler, A. Dlouhy, D.M. Többsen, M. Tovar, Neutron diffraction phase analysis during thermal cycling of a Ni-rich NiTi shape memory alloy using the rietveld method. *Scripta Materialia* **46**, 543–548 (2002)
87. A. Dlouhy, J. Khalil-Allafi, G. Eggeler, Multiple-step martensitic transformations in Ni-rich NiTi alloys — an in-situ transmission electron microscopy investigation. *Phil. Mag.* **83**, 339–363 (2003)
88. E. Hornbogen, Lattice defects and martensitic transformation, in *Micromechanics of advanced materials*, ed. by S.N.G. Chu, P.K. Liaw, R.J. Arsenault, K. Sadananda, K.S. Chan, W.W. Gerberich, C.C. Chau, T.M. Kung (The Minerals, Metals & Materials Society, 1995), pp. 307–315
89. F.C. Lovey, V. Torra, Shape memory in Cu-based alloys: phenomenological behavior at the mesoscale level and interaction of martensitic transformation with structural defects in Cu-Zn-Al. *Progress in Materials Science* **44**, 189–289 (1999)
90. M. Inami, T. Ishii, X. Ren, K. Otsuka, A study of martensitic transformation in Au-51.5at%Cd alloy. in *Materials Science Forum*, (Kanazawa, Japan, 2000), pp. 397–400
91. S. Kustov, J. Pons, E. Cesari, J. Van Humbeeck, Pinning-induced stabilization of martensite PartII. Kinetic stabilization in cu-zn-al alloy due to pinning of moving interfaces. *Acta Mater.* **52**, 3083–3096 (2004)

92. J.I. Pérez-Landazábal, V. Recarte, V. Sánchez-Alarcos, R.G. Leisure, Defect pinning of interface motion in thermoelastic structural transitions of Cu-Al-Ni shape-memory alloy. *Phys. Rev. B* **73**(224101), 1–9 (2006)
93. J.I. Pérez-Landazábal, V. Recarte, V. Sánchez-Alarcos, R.G. Leisure, Defect pinning of interface motion in thermoelastic structural transitions of Cu-Al-Ni shape-memory alloy. *Phys. Rev. B* **73**(224101), 1–9 (2006)
94. F.J. Pérez-Reche, E. Vives, M. Stipich, L. Mañosa, A. Planes, Kinetics of martensitic transitions in Cu-Al-Mn under thermal cycling: Analysis at multiple length scales. *Phys. Rev. B* **69**(64101), 1–7 (2004)
95. M.C. Gallardo, J. Manchado, F.J. Romero, J. del Cerro, E.K.H. Salje, A. Planes, E. Vives, Avalanche criticality in martensitic transition of $\text{Cu}_{67.64}\text{Zn}_{16.71}\text{Al}_{15.65}$ shape memory alloy: A calorimetric and acoustic emission study. *Phys. Rev. B* **81**(174102), 1–8 (2010)
96. J.C. Maxwell, *Capillary Action*. *Encyclopaedia Britannica*. 9th edn (1876)
97. F. Richter, O. Kastner, G. Eggeler, Finite-element model for simulations of fully coupled thermomechanical processes in shape memory alloys. in *ESOMAT 2009*. EDP Sciences (2009)
98. K. Tanaka, S. Kobayashi, Y. Sato, Thermomechanics of transformation pseudoplasticity and shape memory effect in alloys. *Int. J. Plasticity* **2**(1), 59–72 (1986)
99. C. Liang, C. Rogers, One-dimensional thermomechanical constitutive relations for shape memory materials. *J. Intel. Mat. Syst. Str.* **1**, 207–234 (1990)
100. F. Auricchio, A robust integration algorithm for a finite-strain shape-memory-alloy superelastic model. *Int. J. Plasticity* **17**, 971–990 (2001)
101. L.C. Brinson, One-dimensional constitutive behavior of shape memory alloys: Thermomechanical derivation with non-constant material functions and redefined martensite internal variable. *J. Intel. Mat. Syst. Str.* **4**, 229–242 (1993)
102. D. Helm, Formgedächtnislegierungen—Experimentelle Untersuchung, phänomenologische Modellierung und numerische Simulation der thermomechanischen Materialeigenschaften. PhD thesis, (University Kassel, Germany, 2001)
103. C. Müller, O.T. Bruhns, Modelling of polycrystalline shape memory alloys at finite strains based upon the logarithmic stress state. *J. Phys.* **IV**(112), 187–190 (2003)
104. F. Auricchio, L. Petrini, A three-dimensional model describing stress-temperature induced solid phase transformations: solution algorithm and boundary value problems. *Int. J. Numer. Meth. Eng.* **61**, 807–836 (2004)
105. S. Reese, D. Christ, Finite deformation pseudo-elasticity of shape memory alloys—Constitutive modelling and finite element implementation. *Int. J. Plasticity* **24**(3), 455–482 (2008)
106. F. Falk, Model free energy, mechanics and thermodynamics of shape memory alloys. *Acta Metall.* **28**, 1773–1780 (1980)
107. B. Raniecki, C. Lexcellent, Thermodynamics of isotropic pseudoelasticity in shape memory alloys. *Eur. J. Mech. A-Solid* **17**(2), 185–205 (1998)
108. D.C. Lagoudas, Z. Bo, A. Bhattacharyya, A thermodynamic constitutive model for gradual phase transformation of sma materials. in *Mathematics And Control In Smart Structures - Smart Structures And Materials*, ed. by V.V. Varadan, J. Chandra, vol 2715 of *Proceedings of Society of Photo-Optical Instrumentation Engineering (SPIE)*, (SPIE, San Diego, CA, 1996), pp. 482–493
109. R. Heinen, K. Hackl, On the calculation of energy-minimizing phase fractions in shape memory alloys. *Comput. Method. Appl. M.* **196**(21–24), 2401–2412 (2007)
110. I. Müller, A model for a body with shape-memory. *Arch. Ration. Mech. An.* **70**, 61–77 (1979)
111. M. Achenbach, A model for an alloy with shape memory. *Int. J. Plasticity* **5**, 371–395 (1989)
112. I. Müller, S. Seelecke, Thermodynamic aspects of shape memory alloys. *Math. Comput. Model.* **34**, 1307–1355 (2001)
113. S. Seelecke, Modeling the dynamic behavior of shape memory alloys. *Int. J. Nonlin. Mech.* **37**, 1363–1374 (2002)
114. F. Richter, O. Kastner, G. Eggeler, Finite-element simulation of the anti-buckling-effect of a shape memory alloy bar. *J. Mater. Eng. Perform.* **20**, 719–730 (2011) [10.1007/s11665-010-9797-8](https://doi.org/10.1007/s11665-010-9797-8)

115. F. Richter, O. Kastner, G. Eggeler, Implementation of the Müller-Achenbach-Seelecke model for shape memory alloys in ABAQUS. *J. Mat. Eng. Perf.* **18**(5–6), 626–630 (2009) Special issue containing contributions from the Shape Memory and Superelastic Technology Conference, Stresa, Italy, September 21–25 2008
116. F. Richter, Finite-element-simulations of polycrystalline shape memory alloys. In *Smart Structures and Materials and Nondestructive Evaluation and Health Monitoring 2008*, (San Diego, CA, USA, 2008)
117. S. Jaeger, *Experimentelle und theoretische Untersuchungen zu Phasenumwandlungen in NiTi-Bleichen* Master's thesis (Ruhr-University, Bochum, 2010)
118. Y. Xie, Modell zur Simulation einer mehrphasigen Gedächtnislegierung unter mehrachsiger Belastung. PhD thesis, (Technical University of Berlin, 1994)
119. O. Kastner, F. Richter, G. Eggeler, Multivariant formulation of the thermomechanically coupled müller-achenbach-seelecke-model for shape memory alloys. in *Proceedings of the ASME 2009 Conference on Smart Materials, Adaptive Structures and Intelligent Systems*, (ASME, Oxnard, 2009)

First Principles Modelling of Shape Memory Alloys

Molecular Dynamics Simulations

Kastner, O.

2012, XVI, 176 p., Hardcover

ISBN: 978-3-642-28618-6